

6 Combining The Grid and The Skin of The Panel

The panel is formed by attaching the grid layer on the top surface of the skin as shown in Fig. (17). The grid layer is assumed to be perfectly bonded to the skin's surface, meaning the two components do not separate during panel deformations. Accompanying with the classical lamination theory, planes that are perpendicular to the mid-plane of the panel are assumed to remain perpendicular during deformations. This means that in case of bending, in-plane strains vary linearly through the panel's thickness.

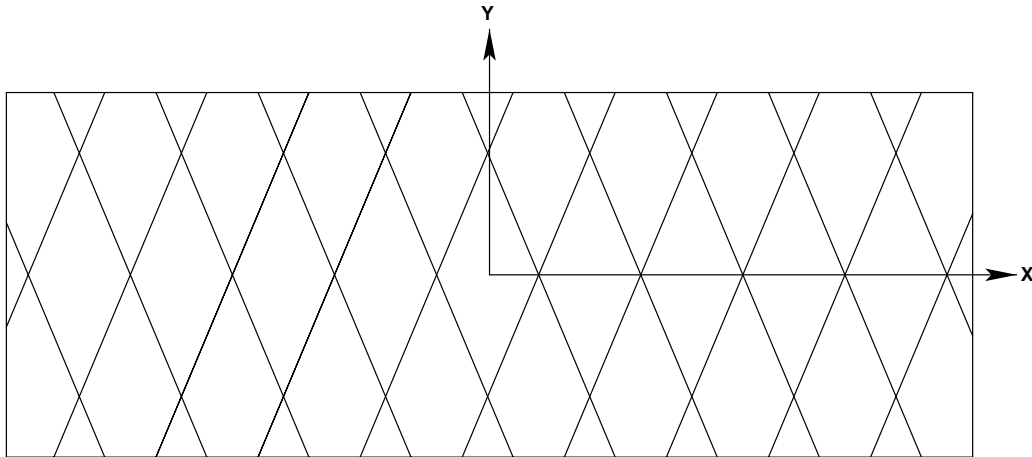


Figure 17: Top View of The Grid

We can consider the smeared grid layer and the skin as two sublaminae forming the panel and treat the panel as a general laminate made of two sublaminae. Furthermore, we can use the constitutive equations that come along with the classical lamination theory to determine the deformations of the panel under different types of loads.

In Chapters 2 and 5, stiffness and thermal properties of the skin and the grid layer were presented respectively. This chapter will introduce how to calculate the panel stiffness properties by using the

stiffness matrices of the skin and the grid layer according to Chapter 4.1. Later, for thermal loading conditions, thermal loads and moments that would act on the panel will be determined by using the free thermal loads acting on the skin and the stiffeners.

Two edge conditions will be considered for the panel; one, when all the edges of the panel are free to deform, and another, when all the edges are restrained, thus suppressing any possible deformations.

When the panel has free-to-deform edges, it can be loaded by both thermal and mechanical loads. Equations will be derived to determine both in-plane and out-of-plane deformations of the panel due to these loads. When the panel is restrained, mechanical loads can not be applied externally, but they may still be experienced by the panel subcomponents in case of a thermal loading. Finally, equations determining these mechanical loads and how they are shared by the skin and the stiffeners will be presented.

To simplify the mechanical and thermal analyses, we want to limit this study to laminates free of any stiffness couplings. Even though the panel may have extension-bending coupling due to its unsymmetric geometry, the skin and the stiffener laminates can be tailored to eliminate their own extension-bending coupling effects. Therefore, in the rest of this document, skin and stiffener laminates will be chosen to have symmetric stacking sequences.

6.1 Mechanical and Thermal Properties of The Panel

In Chapter 4.1, formulas were given to calculate the stiffness matrices, \mathbf{A} , \mathbf{B} and \mathbf{D} of a laminate made of various sublaminates. Once the stiffness matrices for the skin and the smeared grid layer are calculated, stiffness matrices of the panel can be determined by rewriting Eqs. (46), (54) and (55) as;

$$[\mathbf{A}_{ij}] = [\mathbf{A}_{ij}]_s + [\mathbf{A}_{ij}]_r \quad (132)$$

$$[\mathbf{B}_{ij}] = [\mathbf{A}_{ij}]_s \left(\frac{-h_r}{2}\right) + [\mathbf{B}_{ij}]_s + [\mathbf{A}_{ij}]_r \left(\frac{h_s}{2}\right) + [\mathbf{B}_{ij}]_r \quad (133)$$

$$[\mathbf{D}_{ij}] = [\mathbf{A}_{ij}]_s \left(\frac{-h_r}{2}\right)^2 + 2[\mathbf{B}_{ij}]_s \left(\frac{-h_r}{2}\right) + [\mathbf{D}_{ij}]_s + [\mathbf{A}_{ij}]_r \left(\frac{h_s}{2}\right)^2 + 2[\mathbf{B}_{ij}]_r \left(\frac{h_s}{2}\right) + [\mathbf{D}_{ij}]_r \quad (134)$$

Subscripts r and s denote the matrices that belong to the grid layer and the skin respectively, matrices without any subscripts belong to the panel. Since we are considering symmetric skin and stiffener laminates, extension bending coupling stiffness matrices $[\mathbf{B}]_r$ and $[\mathbf{B}]_s$ vanish in above equations. Thus, we rewrite Eqs. (133) and (134) as,

$$[\mathbf{B}_{ij}] = [\mathbf{A}_{ij}]_s \left(\frac{-h_r}{2}\right) + [\mathbf{A}_{ij}]_r \left(\frac{h_s}{2}\right) \quad (135)$$

$$[\mathbf{D}_{ij}] = [\mathbf{A}_{ij}]_s \left(\frac{-h_r}{2}\right)^2 + [\mathbf{D}_{ij}]_s + [\mathbf{A}_{ij}]_r \left(\frac{h_s}{2}\right)^2 + [\mathbf{D}_{ij}]_r \quad (136)$$

It can be seen in Eq. (135) that even if neither the grid layer nor the skin has an extension-bending coupling stiffness matrix, the panel might have one. Existence of coupling between extension and bending suggests that the panel may experience curvatures under in-plane loads.

When a panel with free-to-deform edges undergoes a temperature change, with the temperature distribution being uniform through it's thickness, it experiences strains and possible curvatures. These strains and curvatures can be thought to be caused partly by virtual in-plane loads, also called as thermal loads. Thermal loads acting on the panel can be arranged in a vector form, which is simply the sum of the free thermal load vectors of the skin and the grid layer (Eq. 137).

$$\begin{pmatrix} N_x^T \\ N_y^T \\ N_{xy}^T \end{pmatrix} = \begin{pmatrix} N_x^T \\ N_y^T \\ N_{xy}^T \end{pmatrix}_s + \begin{pmatrix} N_x^T \\ N_y^T \\ N_{xy}^T \end{pmatrix}_r \quad (137)$$

Free thermal loads acting along the edges of the skin and the grid layer create thermal moments with respect to the mid-plane of the panel. Using a vector notation, these thermal moments can be written as;

$$\begin{Bmatrix} M_x^T \\ M_y^T \\ M_{xy}^T \end{Bmatrix} = \begin{Bmatrix} N_x^T \\ N_y^T \\ N_{xy}^T \end{Bmatrix}_r \frac{h_s}{2} - \begin{Bmatrix} N_x^T \\ N_y^T \\ N_{xy}^T \end{Bmatrix}_s \frac{h_r}{2} \quad (138)$$

If there were individual thermal moments acting on the grid layer or on the skin, these moments would have appeared in Eq. (138) as well. But, since we chose the skin layer to be symmetric, there are no thermal moments acting on it under uniform thermal loading. Also, for the grid layer, we are using blade stiffeners that do not experience thermal moments. Therefore, thermal moment terms associated with the skin and the grid layer do not appear in Eq. (138).

So far, the expressions for the stiffness matrices, thermal load and thermal moment vectors of a panel are given. Using these matrices and vectors, an equation system governing the deformations and the mechanical loads experienced by the panel can be introduced. This equation system is,

$$[\mathbf{A}] \begin{Bmatrix} \varepsilon_x^o \\ \varepsilon_y^o \\ \gamma_{xy}^o \end{Bmatrix} + [\mathbf{B}] \begin{Bmatrix} \kappa_x \\ \kappa_y \\ \kappa_{xy} \end{Bmatrix} - \begin{Bmatrix} N_x^T \\ N_y^T \\ N_{xy}^T \end{Bmatrix} = \begin{Bmatrix} N_x^M \\ N_y^M \\ N_{xy}^M \end{Bmatrix} \quad (139)$$

$$[\mathbf{B}] \begin{Bmatrix} \varepsilon_x^o \\ \varepsilon_y^o \\ \gamma_{xy}^o \end{Bmatrix} + [\mathbf{D}] \begin{Bmatrix} \kappa_x \\ \kappa_y \\ \kappa_{xy} \end{Bmatrix} - \begin{Bmatrix} M_x^T \\ M_y^T \\ M_{xy}^T \end{Bmatrix} = \begin{Bmatrix} M_x^M \\ M_y^M \\ M_{xy}^M \end{Bmatrix} \quad (140)$$

Equations (139) and (140) represent 6 equations with 6 unknowns and can be applied to any laminate under combined loading. There are six displacement type (strains and curvatures) and six traction type (mechanical loads and moments) boundary conditions, some of which can be unknowns depending on the boundary conditions. Since, the equation system can be solved for only six un-

knowns, other six of the boundary conditions have to be known parameters. At this point we consider two possibilities for the boundary conditions along the edges of the panel.

6.2 Panel with Free Edges

When the panel does not have any physical restraints along its edges, both mechanical and thermal loads can be applied to it. For a given temperature change and for given in-plane mechanical loads, we can determine the strains and curvatures experienced by this panel by employing the constitutive equations given in Eqs. (139) and (140). Here, the mechanical loads and moments applied to the panel are known apriori and the equation system can be solved for the unknowns of curvatures and mid-plane strains. There are no moments applied on the panel, i.e.,

$$\begin{Bmatrix} M_x^M \\ M_y^M \\ M_{xy}^M \end{Bmatrix} = \begin{Bmatrix} 0 \\ 0 \\ 0 \end{Bmatrix} \quad (141)$$

To calculate the mid-plane strains and curvatures we use,

$$\begin{Bmatrix} \varepsilon_x^o \\ \varepsilon_y^o \\ \gamma_{xy}^o \end{Bmatrix} = [\mathbf{A}_1] \begin{Bmatrix} N_x^M + N_x^T \\ N_y^M + N_y^T \\ N_{xy}^M + N_{xy}^T \end{Bmatrix} \quad (142)$$

$$\begin{Bmatrix} \kappa_x \\ \kappa_y \\ \kappa_{xy} \end{Bmatrix} = [\mathbf{C}_1] \begin{Bmatrix} M_x^T \\ M_y^T \\ M_{xy}^T \end{Bmatrix} \quad (143)$$

where,

$$[\mathbf{D}_1] = [\mathbf{D}] - [\mathbf{B}] [\mathbf{A}^{-1}] [\mathbf{B}] \quad (144)$$

$$[\mathbf{A}_1] = [\mathbf{A}^{-1}] + [\mathbf{A}^{-1}] [\mathbf{B}] [\mathbf{D}_1] [\mathbf{B}] [\mathbf{A}^{-1}] \quad (145)$$

$$[\mathbf{B}_1] = -[\mathbf{A}^{-1}] [\mathbf{B}] [\mathbf{D}_1] \quad (146)$$

$$[\mathbf{C}_1] = [\mathbf{B}_1]^T \quad (147)$$

6.2.1 Load Distribution

Due to the differences in their thermal expansion coefficients and stiffness properties, the skin and the stiffeners may experience mechanical loads and moments during deformations. Whether due to thermal or mechanical loading, these mechanical loads and moments experienced can be calculated after determining the mid-plane strains and curvatures of the panel according to the Eqs. (142) and (143). Mechanical load and moment vectors acting on the skin and the grid layer as a result of panel deformations can be written as,

$$\begin{pmatrix} N_x^M \\ N_y^M \\ N_{xy}^M \end{pmatrix}_{(s,r)} = [\mathbf{A}]_{(s,r)} \begin{pmatrix} \varepsilon_x^o \\ \varepsilon_y^o \\ \gamma_{xy}^o \end{pmatrix} - \begin{pmatrix} N_x^T \\ N_y^T \\ N_{xy}^T \end{pmatrix}_{(s,r)} \quad (148)$$

$$\begin{pmatrix} M_x^M \\ M_y^M \\ M_{xy}^M \end{pmatrix}_{(s,r)} = [\mathbf{D}]_{(s,r)} \begin{pmatrix} \kappa_x \\ \kappa_y \\ \kappa_{xy} \end{pmatrix} \quad (149)$$

Looking at Eq. (149) we can see that none of the panel components experience mechanical moments if the panel does not bend along any direction. Load carried by individual stiffeners can be found as,

$$F_j = A \check{E}_{st} (\cos^2 \phi_j \varepsilon_x + \sin^2 \phi_j \varepsilon_y + \sin \phi_j \cos \phi_j \gamma_{xy}) - F_{st}^T \quad (150)$$

When the panel is bent, strains vary through its thickness. Thus, the longitudinal strain on each stiffener can be written as, $\{\varepsilon\} = \{\varepsilon^o\} + Z_r \{\kappa\}$, where Z_r is the distance between the mid-plane of

the panel and the mid-plane of the grid layer. So, Eq. (150) becomes,

$$F_j = A\check{E}_{st} \left(\cos^2 \phi_j (\varepsilon_x^o + \frac{h_s}{2} \kappa_x) + \sin^2 \phi_j (\varepsilon_y^o + \frac{h_s}{2} \kappa_y) + \sin \phi_j \cos \phi_j (\varepsilon_{xy}^o + \frac{h_s}{2} \kappa_{xy}) \right) - F_{st}^T \quad (151)$$

6.3 Panel With Restrained Edges

A panel with restrained edges under uniform thermal loading can not deform in its plane, and there will be mechanical loads and moments acting along its edges, i.e., reaction forces and moments. Depending on the material properties of the panel and the nature of the thermal loading, these reaction forces can be compressive or tensile. Thus, the nature and the magnitude of these forces determine the type of panel's structural failure.

To determine what kind of loads does a restrained panel experience under uniform thermal loading, we employ the same equations as we did in the previous subsection, i.e., Eqs. (139) and (140).

We know that the mid-plane strains of the panel are zero due to the physical restraints, but we have not specified any conditions about the curvatures at the edges. If we use simply supported edges located at the mid-plane of the panel, curvatures may be observed due to the thermal moments acting on the panel. However, according to a study by A.W. Leissa [21], a laminate under in-plane loads, possessing extension-bending coupling, can be kept flat by appropriate positioning of the simple supports on the out-of-plane axis of the laminate. Since we try to treat the panel as a general laminate, we think this approach can be applied to the grid-stiffened panels as well.

Due to the possibility of contractions under thermal loads, we would like to change the physical character of these simple supports. Here, it is suggested that the supports be like hinges, stretching all along the edges of the panel at the pre-specified locations along the z-axis. Hinge-like simple supports act as revolute joints and do not allow the panel to shrink and loose contact with the fixed edges,

while allowing room for possible curvatures.

We try to preserve the boundary conditions that come along with simply supported edges, because when we get into the buckling analysis in Chapter 6.6 we will see that, this approach eases the modeling of the panel out-of-plane deformations.

Members of the panel, i.e., the skin and the stiffeners, will experience some mechanical loads due to suppression of in-plane strains. These loads can be written by using Eqs. (139) and (140) as,

$$\begin{pmatrix} N_x^M \\ N_y^M \\ N_{xy}^M \end{pmatrix}_{(s,r)} = - \begin{pmatrix} N_x^T \\ N_y^T \\ N_{xy}^T \end{pmatrix}_{(s,r)} \quad (152)$$

the load carried by each stiffener is,

$$F_j = -F_{st}^T \quad (153)$$

Eqs. (152) and (153) suggest that under uniform thermal loading, amount of mechanical loads experienced by the members of a restrained panel are the same in magnitude but opposite in nature as their individual free thermal loads.

If Eqs. (139) and (140) are examined, it can be seen that one of the conditions for the skin or the stiffeners to experience mechanical moments is existence of panel curvatures. We have used the idea that was suggested by Leissa's study and avoided these curvatures. Therefore, no mechanical moments are experienced by the skin or the stiffeners. Another condition for existence of mechanical moments depends on the thermal moments brought along with un-symmetry of the skin and the stiffener laminates. We have already mentioned earlier that, this study does not consider unsymmetric stacking sequences for any of the panel components. As a result, Eqs. (152) and (153) remain intact.

E_{11}	53.3×10^6 Psi
E_{22}	0.73×10^6 Psi
G_{12}	0.76×10^6 Psi
ν_{12}	0.31
α_{11}	-0.64×10^{-6}
α_{22}	17.2×10^{-6}
ply-thickness	5×10^{-3} inches

Table 2: Material Properties of P-100 Graphite Epoxy

6.4 Parametric Studies on The Panel

Thermal expansion coefficients and thermal bending coefficients were demonstrated to be useful for determining a laminate's tendency to expand and bend under thermal loads. Same approach will be applied to the grid-stiffened panels, and plots of how these coefficients vary with respect to the different design parameters will be presented.

The panel in consideration has the same geometric configuration as the panel that was mentioned in the previous sections, i.e., with stiffeners on the top surface, made of balanced-symmetric laminated components and under uniform thermal loading.

Material chosen for these parametric studies is a P-100 graphite epoxy, for which the material properties are presented in Table 2.

6.4.1 Variation of Panel Thermal Expansion Coefficients

A positive (negative) thermal expansion coefficient means that a laminate tries to expand when exposed to a temperature increase (decrease). Higher magnitudes of this coefficient means that the tendency of a laminate to expand or contract is higher. If restrained, this expansion (contraction) be-

havior causes in-plane mechanical loads to be experienced by the laminate. Treating the grid-stiffened panel as a general laminate; we use it's thermal expansion coefficients as indicators of how the in-plane mechanical loads experienced would vary when the panel edges are restrained.

Stiffener stacking sequence is the first parameter we want to treat as a design variable. Here the skin is a quasi-isotropic laminate with the stacking sequence of $[0/\pm 45/90]_s$ and the stiffeners have the varying stacking sequence of $[\pm\theta]_s$. The stiffeners are oriented by ± 30 degrees from the x-axis of the panel and their height is 0.5 inches. Fig. (18) shows the variation of panel thermal expansion coefficients along x and y axes with respect to θ , the ply-angle of the stiffener laminates. The skin itself has a negative thermal expansion coefficient of -3.28×10^{-7} along both panel axes. For $\theta = 0$, the stiffeners have negative longitudinal thermal expansion coefficient too, so at this point the panel has a negative thermal expansion coefficient along both axes. As the ply-angle θ starts increasing, thus causing the longitudinal expansion coefficient of the stiffeners to increase, the thermal behavior of the panel changes from contraction to expansion. Looking at the graph, we see that there is a minimum for both of the panel thermal expansion coefficients (α_x and α_y). This minimum, where the panel has the highest tendency to contract along both panel axes, corresponds approximately to 30 degrees. After this point both thermal expansion coefficients start increasing. At 45 degrees they are equal to each other and right after 45 degrees they cross the zero coefficient line ($\alpha = 0$). However, upon zooming into the graph it was seen that they did not intersect the zero coefficient line at the same point which means design of a panel that would not expand along any of the axes is not possible. For stiffener ply-angles greater than approximately 48 degrees, the panel tries to expand, and for ply-angles less than approximately 45 degrees, the panel tries to contract along both axes. So, keeping θ within this interval can help to minimize the panel deformations, and in case of restrained edges, can minimize the mechanical loads that would act on the panel.

Fig. (19) shows how the grid height contributes to the in-plane expansion coefficients of the panel. Except the stiffener stacking sequence and the grid height, the panel considered here has the same configuration as the panel that was used to plot the previous graph. Here, the stiffeners have the stacking sequence of $[\pm 20]_s$ and their height is variable. It is seen that as the height of the grid-layer increases, coefficients of thermal expansion along both panel axes drops from the skin's thermal expansion coefficient value ($\alpha_x = \alpha_y = -3.28 \times 10^{-7}$ at $h_r = 0$), to the values of -1.5×10^{-6} and -1.82×10^{-6} along the x and y axes respectively. The plots of α_x and α_y seem not to vary considerably after the grid height reaches 0.5 inches. This feature could be used to change the stiffness properties of the panel while keeping the thermal loads almost constant along it's edges.

Next we would like to see the effect of stiffener orientations on the thermal expansion behavior of the same panel configuration. Fig. (20) shows the variation of α_x and α_y of the panel versus the stiffener orientations. It can be seen that, when the stiffeners are all parallel to the x-axis of the panel (when $\phi = 0$); thermal expansion coefficient along the panel y coordinate axis is positive, indicating an expansion, and the expansion coefficient along the x-axis is negative, indicating a contraction. As the stiffener orientation starts increasing, value of both α_x and α_y show a drop till the orientation reaches about 20 degrees. During this drop, the tendency of the panel along the y-axis changes from expansion to contraction, going through zero expansion point ($\alpha_y = 0$) in between. Now the panel tries to contract along both axes. As we can see, changing the stiffener orientation not only changes the magnitude of panel thermal expansion coefficients, but also changes their nature. This suggests that, we may be able to get a desired thermal response from the panel along both axes by changing the stiffener orientations.

Variations of the panel thermal expansion coefficients with respect to the skin stacking sequence are shown in Fig. (21). Here the skin has a stacking sequence of $[0/\pm\theta/90]_s$. When θ in skin stacking

sequence is 0 degrees, panel thermal expansion coefficient along the x-axis is -8.353×10^{-7} and the thermal expansion coefficient along the y-axis is -3.764×10^{-6} . As the variable ply angle increases, expansion coefficients of the panel along the x and y-axes decrease and increase respectively. From 0 degrees to 20 degrees, the thermal expansion coefficients of the panel do not show any change in their values. Between 20 and 50 degrees there is considerable change and for ply angles greater than 50 degrees, values of the thermal expansion coefficients remain steady, i.e., $\alpha_x = -1.5737 \times 10^{-6}$ and $\alpha_y = -1.2817 \times 10^{-6}$. Now we see a situation where the thermal expansion coefficients of the panel do not change for certain values of a design parameter. Although changing the skin stacking sequence might not change the expansion coefficients in certain intervals of θ , other properties like in-plane stiffness and bending stiffness of the panel do change. This feature could be useful if one was trying to keep the thermal expansion coefficients of the panel constant while trying to obtain certain panel stiffness properties.

For the panel configuration specified here, one can roughly comment on the dependence of panel thermal expansion coefficients on one of the design variables at a time. If two or more design variables are varied at the same time, variation of panel in-plane response becomes very complicated and it is not possible to lay out a general discussion to predict this response. However, graphs presented in this chapter will be useful in terms of forming our basis on predicting how certain variables may effect the deformation response of the panel.

6.4.2 Variation of Panel Thermal Bending Coefficients

Thermal bending coefficient indicates the tendency of a laminate to bend under thermal loads. A positive (negative) thermal bending coefficient means that the panel tends to bend concave down (up), i.e., the stiffeners on top being stretched (compressed) and the skin being compressed (stretched).

Variations in thermal bending coefficients help us to see the variations of mechanical moments that would act on a panel if it's edges were restrained during thermal loading. So, here we will try to explain the relations between the thermal bending coefficients and the possible panel design parameters by using graphs.

Starting with the stiffener laminate stacking sequence as our first design parameter, we chose a panel with stiffeners on it's top surface. The stiffeners are oriented by ± 30 degrees and have stiffener height of 0.5 inches. The skin and the stiffener laminates have the stacking sequences of $[0/\pm 45/90]_s$ and $[\pm\theta]_s$ respectively. Fig. (22) shows the variation of thermal bending coefficients, ξ_x and ξ_y with respect to the θ in the stiffener stacking sequence.

When the stiffeners are all made of 0 degree plies, the panel has negative curvatures along both axes, thus in a concave up shape. This is simply because the stiffeners try to shrink at a greater rate than the skin does along both panel axes. As θ increases, thermal bending coefficients of the panel increase, both of them reaching a local maximum around $\theta = 28$. Increasing θ furthermore decreases the magnitude of the coefficients and causes the two lines to intersect each other and the zero curvature line, ($\xi = 0$) at $\theta = 45$. This is noteworthy because at $\theta = 45$ the grid-layer has the same thermal expansion coefficients as the skin does and, therefore the panel does not experience any bending. For θ values greater than 45 degrees, the grid-layer starts having larger thermal expansion coefficients than the skin, and this causes the panel to acquire a concave down shape, i.e., positive curvature along both axes.

Height of the grid-layer, h_r , also effects the thermal bending coefficients of the panel as illustrated in Fig. (23). To plot this graph, same panel configuration is chosen as the panel mentioned previously, only differences being the stiffener stacking sequence and the grid height. Here, all the stiffeners have the stacking sequence of $[\pm 20]_s$ and their height is not fixed. It can be seen that as the grid height

increases, both thermal bending coefficients increase rapidly in magnitude to a maximum at around 0.2 inches. After this maximum, the coefficient magnitudes show a smooth decline with increasing h_r . Thermal bending coefficients appear on the negative region of the graph at all times indicating a concave up shape. This graph may suggest that the height of the grid-layer does not effect the nature of the concavity of the panel, but effects it's magnitude. Depending on the stiffener longitudinal expansion coefficient thus depending on the stiffener stacking sequence, these plots could have been in the positive part of the graph as well, indicating a concave down geometric shape. What is important in this graph is that neither of the coefficients cross the zero bending coefficient ($\xi = 0$) line, meaning that changing the grid height does not change the concavity of a panel under uniform thermal loading.

Changing the orientations of the stiffeners have considerable impact on thermal bending of the panel. Using the same panel configuration, we would like to vary the stiffener orientations and see their effect on the thermal bending coefficients, ξ_x and ξ_y . The output is presented in Fig. (24), with the x-axis being the stiffener orientation θ . When all the stiffeners are parallel to the x-axis of the panel, $\phi = 0$, the panel tries to bend concave up along the x-axis with a bending coefficient of -4.675×10^{-6} and tries to bend concave down along the y-axis with a bending coefficient of 3.338×10^{-6} . We see that as θ increases, both ξ_x and ξ_y change in nature and in magnitude. For certain intervals of stiffener ply angle θ , the panel tends to bend concave up along both axes and in certain intervals it just tends to bend into the shape of a saddle. We can conclude that when the skin and the grid-layer have different thermal expansion coefficients, the stiffener orientations can be adjusted to get a certain bending behavior from the panel.

6.5 Conclusions On Panel Thermal Behavior

We have tried to find ways to relate the deformations and design parameters of panels under uniform thermal loading. Panel design parameters are;

- Stiffener stacking sequence,
- Stiffener orientations,
- Grid height,
- Skin stacking sequence

For specific configurations in which only one design parameter is varied, the graphs presented in this section can be used to analyze the panel's thermal responses. Changing more than one design parameter at a time requires contour plots and upon plotting them it is seen that there is no direct relation that can be stated between the varied parameters. However, based on the plots presented in this section certain conclusions can be drawn.

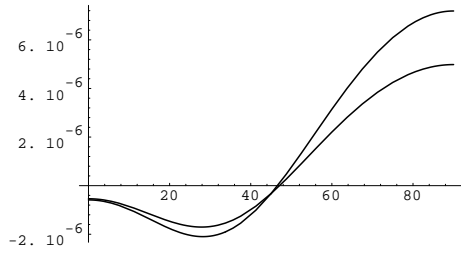
Stiffener stacking sequence effects the stiffness and thermal properties of the stiffeners, the grid-layer and the panel. Varying the stiffener stacking sequence allows us to change the longitudinal thermal expansion coefficient of every stiffener, which in turn helps us manipulate the thermal expansion and bending behavior of the panel. As was mentioned earlier, when the stiffener stacking sequence is chosen in such a way that the grid-layer and the skin have the same thermal expansion coefficients along both panel axes, the panel remains flat under uniform thermal loads.

Stiffener orientations do not affect the individual properties of the stiffeners but the properties of the grid-layer along the panel coordinate axes. Varying the stiffener orientations changes the nature of panel thermal expansions, i.e., panel can be made to contract along both coordinate axes or to expand

along one, while contracting along the other. However, as illustrated in Fig. (20) and Fig. (24), getting the exact desired behavior from the panel by varying this parameter may not be very straightforward.

Changing the height of the grid-layer changes the thermal moments and loads which determine the curvatures and strains along the edges of the panel. Stiffener height does not effect the thermal or stiffness properties of the individual stiffeners, but effects the load shared by the skin and the grid-layer. Even though the magnitudes of panel curvatures depend on the grid-height, it is seen that their nature does not change by varying this parameter.

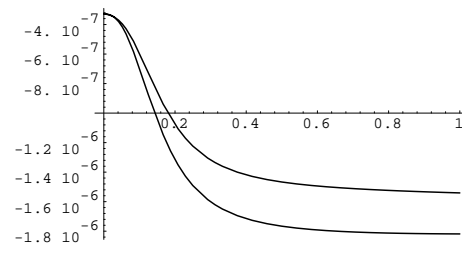
Skin stacking sequence has a similar influence over the panel behavior as the stiffener stacking sequence. Changing the skin stacking sequence effects stiffness and thermal properties of the panel, which in turn changes the deformation response and the load distribution between the skin and the stiffeners.



θ

α

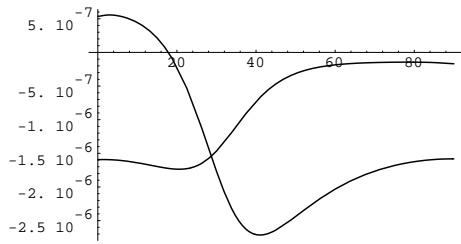
Figure 18: Thermal expansion coefficients vs stiffener ply angle θ



h_r

α

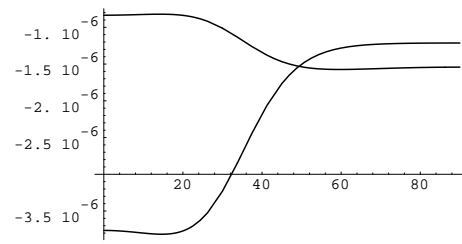
Figure 19: Thermal expansion coefficients vs grid height



ϕ

α

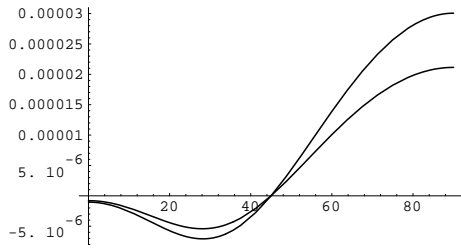
Figure 20: Thermal expansion coefficients vs stiffener orientation ϕ



θ

α

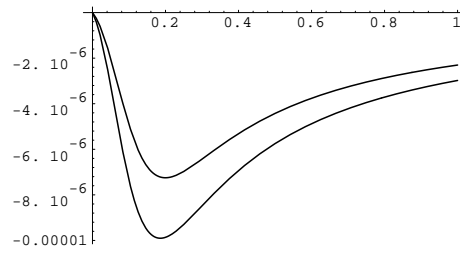
Figure 21: Thermal expansion coefficients vs skin ply angle θ



θ

ξ

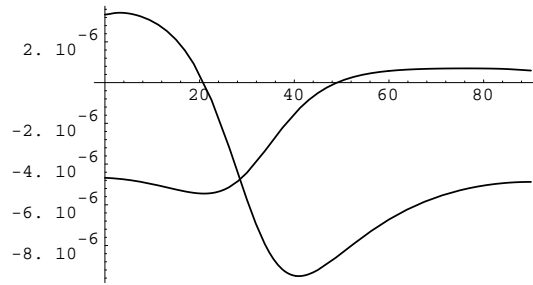
Figure 22: Thermal bending coefficients vs stiffener ply angle θ



h_r

ξ

Figure 23: Thermal bending coefficients vs grid height



ϕ

ξ

Figure 24: Thermal bending coefficients vs stiffener orientation ϕ

6.6 Stability of The Panel Under Thermo-mechanical Loads

Major objective beneath employing grid-stiffeners in a panel is to reduce the weight of the panel structure. Unfortunately, reduced weight can sometimes bring reduced structural stability. Therefore, grid-stiffened panels may fail due to loss of stability under various types of loads. This part of the study aims to describe the methodology that is followed in formulating the stability analysis of a grid-stiffened panel under thermal loading.

To briefly define our problem; we would like to carry out the buckling analysis of a grid-stiffened panel with stiffeners on one side under uniform thermal loading. The panel is restrained along all of its edges with hinge-like supports that were described in Chapter 6.3. The stiffeners are assumed to carry loads which are applied at their end-points and they are assumed to be flexible at their intersection points with the other stiffeners. Here, we would like to determine the relationship between the thermal load i.e., temperature difference applied to the panel, that causes panel buckling and the different panel design variables.

As was stated previously, a grid-stiffened panel consists of several components, the skin and the stiffeners. While carrying out the stability analysis of the panel, these components' stability criteria will be handled separately. Since the skin and the stiffeners are all made of composite laminates, their individual buckling analyses will be the same as of a general laminate's. For the buckling analysis separate out-of-plane deflection functions will be assumed for each member. To ensure continuity of deflection and of surface slopes at the grid-skin interface, constraints will be built into the problem at number of discrete points along the stiffeners' longitudinal axes. So, the problem will have two constraints associated with the physical continuity of the panel at the interface of the two components. An additional constraint is also introduced into the problem to consider material failure of panel

members according to the first ply strain failure theory. It should be noted that the latter constraint is completely different in nature than the grid-skin interface continuity constraint.

It is assumed that in case of buckling, the panel will fail in a bifurcation mode and there will be no deformations during the pre-buckling stage. Relying on the results presented in the literature by various scholars [9], [10], Rayleigh-Ritz method is chosen to carry out the buckling analyses of the panel.

6.6.1 Rayleigh-Ritz and Lagrange Multiplier Methods

Ritz method is a convenient way to obtain approximate solutions to boundary value problems. This approach is applicable to bending, buckling and free vibration problems. All of these problems are governed by a total energy condition, in which the total energy of the structure needs to be at its minimum value for structural equilibrium. For buckling problem of a laminate under in-plane loads with no vibration or transverse loads, the total energy is defined as the sum of the strain energy stored in the body added to the potential energy of the external forces. To comply with one of Ritz method's requirements, an out-of-plane deflection function satisfying the laminate kinematic boundary conditions is assumed and substituted into the energy expressions.

In our problem we sum up the total energies of the skin and of all the stiffeners to form the total energy of the panel, and we assume double sine Fourier series for each member's out-of-plane deflection function. Assumed out-of-plane functions satisfy the boundary conditions given in Chapter 6.3, thus complying with the Rayleigh-Ritz method's requirement. Before going into the minimization of the panel's total energy, we would like to incorporate the afore mentioned skin-grid interface deformation continuity constraints into the problem, for this purpose we suggest using Lagrange multiplier method. More detailed discussion on Rayleigh-Ritz method can be found in the literature [17].

Lagrange multiplier method (LMM) is a practical method to minimize continuous objective functions with equality constraints imposed on them. It basically tries to minimize a function, called the Lagrangian, which consists of summation of the original objective function (panel total energy) with the constraint functions multiplied with distinct Lagrange multipliers. Minimization of the Lagrangian requires all its first order derivatives with respect to the objective function variables and with respect to the Lagrange multipliers to be zero. As a result, this method leads to a number of equations with the same number of unknowns which need to be solved simultaneously. More discussion on this topic can also be found in the literature [18], [10].

6.6.2 Energy Expressions of A Laminate

Here, we present the strain energy and potential energy expressions of a composite laminate under in-plane loading with no vibration or transverse loads. As given in references [17] and [16], we would like to include the expansion strains due to uniform thermal loads into these expressions as well.

Rewriting the stress-strain relationships for a fiber reinforced composite ply we get,

$$\sigma_i = \sum_{j=1,2,6} [\bar{\mathbf{Q}}]_{ij} (\varepsilon_j - \varepsilon_j^T) \quad (154)$$

where $[\bar{\mathbf{Q}}]_{ij}$ is the transformed stiffness matrix for any angle ply, and ε_j^T is the transformed thermal strain vector that was defined in Eq. (4). Strain energy expression of a laminate in the presence of expansion (thermally induced) strains is as follows;

$$\mathbf{U} = \frac{1}{2} \int \int \int [\sigma_x(\varepsilon_x - \varepsilon_x^T) + \sigma_y(\varepsilon_y - \varepsilon_y^T) + \sigma_z(\varepsilon_z - \varepsilon_z^T) + \sigma_{xy}(\varepsilon_{xy} - \varepsilon_{xy}^T)] dx dy dz \quad (155)$$

Since through the thickness strain is neglected in our model, third term in the triple integration will vanish. It should be noted that the strain energy is written in terms of mechanical strain, i.e., the difference between total strain and expansion strain. These are the strains that produce stress.

Free expansion does not induce stress over the laminate. Taking the stress-strain relations written in Eq. (154) and substituting into Eq. (155) we get,

$$\begin{aligned} \mathbf{U} = & \frac{1}{2} \int \int \int \left[[\bar{\mathbf{Q}}]_{11}^k (\varepsilon_x - \varepsilon_x^{kT})^2 + [\bar{\mathbf{Q}}]_{22}^k (\varepsilon_y - \varepsilon_y^{kT})^2 + 2 [\bar{\mathbf{Q}}]_{12}^k (\varepsilon_x - \varepsilon_x^{kT}) (\varepsilon_y - \varepsilon_y^{kT}) + \right. \\ & \left. 2 [\bar{\mathbf{Q}}]_{16}^k (\varepsilon_x - \varepsilon_x^{kT}) (\varepsilon_{xy} - \varepsilon_{xy}^{kT}) + 2 [\bar{\mathbf{Q}}]_{26}^k (\varepsilon_y - \varepsilon_y^{kT}) (\varepsilon_{xy} - \varepsilon_{xy}^{kT}) \right] dx dy dz \end{aligned} \quad (156)$$

Substituting the strain-displacement relations and laminate stiffness matrices into the strain energy we obtain a double integral in the form,

$$\begin{aligned} \mathbf{U} = & \frac{1}{2} \int \int \left\{ A_{11} \left(\frac{\partial u^o}{\partial x} \right)^2 + 2 A_{12} \left(\frac{\partial u^o}{\partial x} \frac{\partial v^o}{\partial y} \right) + A_{22} \left(\frac{\partial v^o}{\partial y} \right)^2 + \right. \\ & 2 \left(A_{16} \frac{\partial u^o}{\partial x} + A_{26} \frac{\partial v^o}{\partial y} \right) \left(\frac{\partial u^o}{\partial y} + \frac{\partial v^o}{\partial x} \right) + A_{66} \left(\frac{\partial u^o}{\partial y} + \frac{\partial v^o}{\partial x} \right)^2 - 2 N_x^T \frac{\partial u^o}{\partial x} - \\ & 2 N_y^T \frac{\partial v^o}{\partial y} - 2 N_{xy}^T \left(\frac{\partial u^o}{\partial y} + \frac{\partial v^o}{\partial x} \right) - B_{11} \frac{\partial u^o}{\partial x} \frac{\partial^2 w}{\partial x^2} - 2 B_{12} \left(\frac{\partial v^o}{\partial y} \frac{\partial^2 w}{\partial x^2} + \frac{\partial u^o}{\partial x} \frac{\partial^2 w}{\partial y^2} \right) - \\ & B_{22} \frac{\partial v^o}{\partial y} \frac{\partial^2 w}{\partial y^2} - 2 B_{16} \left[\frac{\partial^2 w}{\partial x^2} \left(\frac{\partial u^o}{\partial y} + \frac{\partial v^o}{\partial x} \right) + 2 \frac{\partial u^o}{\partial x} \frac{\partial^2 w}{\partial x \partial y} \right] - 2 B_{26} \left[\frac{\partial^2 w}{\partial y^2} \left(\frac{\partial u^o}{\partial y} + \frac{\partial v^o}{\partial x} \right) + \right. \\ & \left. 2 \frac{\partial v^o}{\partial y} \frac{\partial^2 w}{\partial x \partial y} \right] - 4 B_{66} \frac{\partial^2 w}{\partial x \partial y} \left(\frac{\partial u^o}{\partial y} + \frac{\partial v^o}{\partial x} \right) + D_{11} \left(\frac{\partial^2 w}{\partial x^2} \right)^2 + 2 D_{12} \frac{\partial^2 w}{\partial x^2} \frac{\partial^2 w}{\partial y^2} + \\ & D_{22} \left(\frac{\partial^2 w}{\partial y^2} \right)^2 + 4 \left(D_{16} \frac{\partial^2 w}{\partial x^2} + D_{26} \frac{\partial^2 w}{\partial y^2} \right) \frac{\partial^2 w}{\partial x \partial y} + 4 D_{66} \left(\frac{\partial^2 w}{\partial x \partial y} \right)^2 + 2 M_x^T \frac{\partial^2 w}{\partial x^2} + \\ & \left. 4 M_{xy}^T \frac{\partial^2 w}{\partial x \partial y} + 2 M_y^T \frac{\partial^2 w}{\partial y^2} \right\} dx dy + \int \int \left[\int_{-h/2}^{h/2} f(Q_{ij}^k, \varepsilon_i^{T^k}) dz \right] dx dy \end{aligned} \quad (157)$$

and,

$$\begin{aligned} f(Q_{ij}^k, \varepsilon_i^{T^k}) = & Q_{11}^k (\varepsilon_x^{T^k})^2 + 2 Q_{12}^k \varepsilon_x^{T^k} \varepsilon_y^{T^k} + 2 Q_{16}^k \varepsilon_x^{T^k} \varepsilon_{xy}^{T^k} + 2 Q_{26}^k \varepsilon_y^{T^k} \varepsilon_{xy}^{T^k} + Q_{22}^k (\varepsilon_y^{T^k})^2 + \\ & Q_{66}^k (\varepsilon_{xy}^{T^k})^2 \end{aligned}$$

where k denotes the k -th layer.

What makes this strain energy equation different from that of a panel under pure mechanical loading is the presence of free thermal loads and moments denoted with the superscript T . For the

symmetric laminates we use for the skin and for the stiffeners, extension-bending stiffness coupling matrix terms and the free thermal moments given in Eq.(157) are zero. It should be noted that if the thermal load was nonuniform, free thermal moments would remain in the above expression. Also, when mid-plane deflections are assumed to be constant in the plane of the mid-plane, all the partial derivatives including terms u^o and v^o vanish as well. Last term involving the double integral is independent of the out-of-plane deflection of the laminate, so although it contributes to the total strain energy, it has no effect on the buckling analysis.

It should be noted that the strain energy obtained for a laminate under uniform thermal loading subject to the mentioned assumptions does not have any terms dependent on the thermal load. So, we can say that the strain energy expression needed for our problem will be exactly the same as the expression used in Gürdal and Grall's study [10].

Although the strain energy is seen not to depend on the free thermal loads, potential energy of a laminate may depend on them through the relations defined between the mechanical and thermal loads (see Chapter 6.3). We can simply write the potential energy of a laminate as;

$$V = \frac{1}{2} \int \int \left[N_x \left(\frac{\partial w}{\partial x} \right)^2 + N_y \left(\frac{\partial w}{\partial y} \right)^2 + 2 N_{xy} \frac{\partial w}{\partial x} \frac{\partial w}{\partial y} \right] dx dy \quad (158)$$

Summing up the strain energy \mathbf{U} and potential energy \mathbf{V} we get the total energy $\mathbf{\Pi}$ that needs to be minimized to satisfy the stability criterion.

In Gürdal and Grall's study [10], a model to carry out the buckling analysis of the same panel configuration under mechanical loads was given. For the panel considered in this study, i.e., a panel under uniform thermal loading with four restrained edges, the total energy expression of the structure is the same as the expression given in that study [10]. Therefore, derivations of the buckling problem equations will not be presented in this chapter and the reader is strongly advised to refer to the study

by B. Grall and Z. Gürdal.

7 Fortran Code SPANDO

SPANDO (Stiffened Panel Design and Optimization) is a Fortran 77 code which is developed by the Virginia Tech Engineering Science and Mechanics Dept. to design and optimize grid-stiffened panels that are under mechanical loads.

SPANDO employs Lagrange Multiplier Technique to predict the critical buckling loads and modal shapes of grid-stiffened panels. It may also be coupled with ADS (Automated Design Synthesis), a numerical optimizer used to determine minimum weight or minimum cost designs subject to constraints on buckling of the panel assembly and material strength failure. A maximum strain criterion is used to determine material failure in both the skin and the stiffeners. The combination of SPANDO and ADS provides a powerful yet computationally efficient tool in the initial design stages of grid-stiffened composite panels and can reduce the dependence on computationally intensive analysis methods (such as finite elements) in the overall design of such structures.

A grid-stiffened panel is comprised of both a skin and a grid of stiffeners that may be placed on one or both sides of the skin. A typical grid stiffened panel is shown in Fig. (13). It is assumed that the load is applied to the stiffeners only at the ends of the stiffeners along their longitudinal axes. The lay-ups of both the skin and the stiffeners are assumed to be symmetric and balanced, eliminating bending-extension coupling and shear-extension coupling.

All stiffeners have the same lay-up, thickness, and height and can be oriented in any direction subject to following restrictions:

- All diagonal stiffeners occur in equal but opposite pairs
- The stiffener network is symmetric with respect to the panel centerlines.

These restrictions insure that extension-shear coupling terms are eliminated for the overall panel.

Furthermore, if all the equal and opposite stiffener pairs are at a single orientation, then the Poisson stiffness terms are equivalent. If stiffeners are placed on only one side of the skin then the grid-stiffened panel is no longer symmetric and may exhibit some bending-extension coupling.

7.1 Modifications on SPANDO

A part of this study was to modify the SPANDO to enable the code to analyze the thermal loading effects on the grid-stiffened panels.

We are interested in calculating the deformations of a panel under both mechanical and uniform thermal loads by using the classical lamination theory. The original code was capable of calculating in-plane deformations of the panel but not the curvatures and, it did not treat the thermal loading effects on the panel either. The modifications that are undertaken as a result of this analytical study includes calculation of in-plane strains and curvatures of the panel under both uniform thermal loads and mechanical loads. As a result of the deformations and the thermal loads, stresses may be experienced by various members of the panel, and the code is changed to calculate these stresses as well.

Two boundary conditions are considered, either all the panel edges are free to deform or they are all restrained. In both cases various mechanical loads may be experienced by the skin and by the stiffeners. For the first case the code calculates these mechanical loads by using panel deformations, and thermal and stiffness properties of the subcomponents. In the second case, due to the suppression of the deformations these mechanical loads are calculated by using the thermal and stiffness properties of the skin and the stiffeners.

Minor changes are done in the input file for the integration of the mentioned changes into the SPANDO. After the lines where mechanical loads are defined, a line depicting the temperature differ-

ence is introduced and stored under the variable name DELT in the input file. If this variable is seen to have a zero value, the code skips all the steps associated with thermal loading.

Two more input parameters, namely longitudinal and transverse thermal expansion coefficients of the skin and stiffener materials are added along with the rest of the material properties.

The original code used the input parameter NEPSX to determine the panel boundary condition in the x direction. In the modified version of the code, another parameter, NEPSY is introduced to perform the same function along the y-axis, but the functions of these parameters are changed slightly. Now, NEPSX and NEPSY determine the boundary conditions in the x and y coordinates of the panel respectively, where an integer value of 1 denotes a free edge and a 0 means a simply supported edge.

A copy of the modified input file is presented in Appendix C with all the necessary explanations.

7.2 Verification Studies

After making the necessary changes in SPANDO, several cases are analyzed for which the panel responses may be predicted apriori. The output of these cases are examined to assure the accurate execution of the code.

First of these cases is a panel under pure thermal loading with all free edges. The panel has stiffeners on only one side of the skin and both the skin and the stiffeners are made of the same material with the same stacking sequence of $[0/90]_{n_s}$. Stacking sequence of $[0/90]_{n_s}$ creates in-plane orthotropy for the skin, causing the thermal expansion coefficient of the skin along x and y axes to be the same. Same material and same stacking sequence suggests that the skin and the stiffener laminates have the same thermal expansion coefficients along their material directions. So, as a result, both the skin and the grid layer try to deform at the same rate along both panel directions when exposed to a uniform thermal load. When all the layers of a panel have the same thermal expansion coefficient in

both panel directions, such as in this case, the panel is expected not to bend under uniform thermal loads. Looking at the output file of the first case we see that this holds true. The panel experiences contraction in all the material directions and the curvatures come out as zero.

Second case consists of a panel with stiffeners on one side of the skin and placed parallel to the x-axis of the panel. Both the skin and the stiffeners are made of the same material with all 0 degree plies. Expected response of this panel under a uniform thermal load is expansion along the panel y-axis and contraction along the x-axis without any curvatures. The deformation along the y-axis should not be affected by the presence of the stiffeners since; the stiffeners are all parallel to the x-axis and they do not contribute to any of the panel's properties along the y-axis. So, the strain observed along the y-axis under uniform thermal loading should be equal to the product of the skin's transverse thermal expansion coefficient and the induced temperature change. Transverse thermal expansion coefficient of the selected skin material is 17.2×10^{-6} and the applied temperature difference is 200 degrees. We see that their product is 3.44×10^{-3} which is the same value obtained in the output file for panel strain along the y-axis. Likewise we obtain the panel strain along the x-axis as -1.28×10^{-4} which is the product of -0.64×10^{-6} , (α_{11}) and 200 degrees, (ΔT) . This panel configuration remains flat during thermal deformation because, the grid layer has the same expansion coefficient with the skin along the x-axis of the panel and the grid layer does not possess thermal expansion coefficient or stiffness along the y-axis. The expansion of the skin along the y-axis is not under any effect from the stiffeners and therefore the skin expands without any curvature in this direction.

Third case consists of a panel with stiffeners that are on both sides of the skin and the panel dimensions are 70 inches by 70 inches. We choose the stiffener laminates to be all 0 degree plies. To obtain an in-plane orthotropic behavior from the grid layer, we design the stiffeners to have the orientations of 45 and -45 degrees, forming a symmetric layer with respect to the x and y axes. We

would like the skin to be orthotropic too, so we choose $[0/\pm 45/90]_{2s}$ for its stacking sequence. Finally as a consequence of these orthotropic layers, we expect the panel to experience the same amount of strain along both x and y axes with no bending effects. In the output file of this case we see that the panel contracts at a rate of 7.58889×10^{-5} along both directions with zero curvature, thus verifying our expected results.

Next we would like to see if the loads experienced by the skin and the stiffeners in this panel configuration are calculated accurately by SPANDO. This is why we chose the stiffener laminates to have a different stacking sequence than of the skin's. Different stacking sequences create different thermal expansion coefficients in the members. Although the panel is free to deform along its edges, the difference between the skin's and the stiffeners' thermal expansion coefficients is expected to create loads on the two layers upon thermal loading.

Looking at the output file, we see that the stiffeners and the skin do experience finite amounts of mechanical loads. Furthermore, when we compare the coefficient of thermal expansion of the stiffeners and of the skin, we see that the stiffeners try to contract at a greater rate than the skin does. So, upon thermal loading, this causes the stiffeners to be stretched by the skin and the skin to be compressed by the stiffeners. The panel, however, does not experience bending because of symmetric placement of the grid on both sides of the skin. Positive and negative quantities in the output files refer to the strains and stresses that are due to compression and tension respectively.

Fourth case is similar to the second (stiffeners on one side of the panel, placed parallel to the panel's x-axis), with the only difference being the stacking sequence of the skin, $[90]_{16}$ instead of $[0/90]_{2s}$. Because the skin has all 90 degree plies, upon thermal loading it tries to expand along the x-axis and shrink along the y-axis. But the stiffeners which are all along the x-axis try to shrink as well. So, along the x-axis we have a skin that is trying to expand and a series of stiffeners on the top

trying to contract. This is expected to create curvature along the x-axis. On the other hand, because the grid layer does not have any thermal or stiffness properties along the y-axis, we expect the panel to remain flat along this axis. When we have a look at the output file provided for this case, there is a curvature of -1.15361×10^{-3} along the x-axis and a curvature of 4.87968×10^{-6} along the y-axis. Even though the latter curvature is not zero, it is negligible when compared with the curvature along the x-axis.

All four cases that are given above are also tested on a Mathematica program written to carry out the pre-buckling deformation analysis of grid-stiffened panels. It was seen that results obtained by SPANDO were also in agreement with the results obtained from the Mathematica code.

7.3 Convergence Study For SPANDO Parameters

As it is for most studies in which double sine series are involved, there is a real need to know the lowest number of terms that will give a good approximation of the solution. It should be recalled that the Fourier series approach relies on infinite sums of terms, and that the precision increases with the number of terms in the series. These terms are written in matrix form in the computer code, and the more they are the larger is the order of the system and the time to solve it; but the better is the precision of the result.

With the Lagrange multiplier technique, constraints are imposed at certain points along the length of the stiffeners. This technique results in adding as many supplementary equations as the number of constraint points. However, a large number of constraint points will increase the order of the system. For this reason, the minimum number of constraint points that are needed to obtain a reasonable solution should be determined.

If the number of constraint points corresponding to a continuous constraint is small, the system will be under restrained, and in the case of buckling response, the system will buckle in a mode that violates the constraint conditions of the actual system. This is important for the determination of the buckling load of such a system since the determined buckling load will be lower than the actual. This leads to a conservative design.

In the case of the geodesically stiffened panel, there are 4 parameters that need to be studied.

M : number of terms for the skin deflection along the x axis.

N : number of terms for the skin deflection along the y axis.

K': number of terms for the stiffener deflection along the η axis.

K : number of constraint points per stiffener.

The aim of the following convergence study is to show the influence of the different parameters on the resulting critical load of the panel. This study was done on a panel with 10 stiffeners that were oriented by ± 39 degrees from the x-axis of the panel, with the stiffeners being on one side of the panel only. Top view of this panel is given in Fig. (25). The plots of this convergence study are obtained by varying one parameter at a time while keeping all the other convergence parameters constant. Constant values of these parameters are, $M = 25$, $N = 18$, $K = 16$, $K' = 5$.

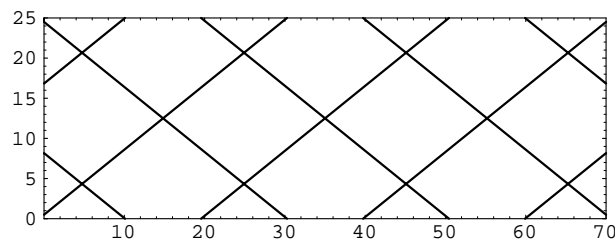


Figure 25: Top view of the panel used for the convergence study

7.3.1 Influence of M and N

M and N correspond to the number of terms in the skin deflection series along x and y axes. Setting them to small numbers decreases the degree of freedom of the skin, making it behave more rigid than it normally is. This causes the eigenvalue of the system to be higher than its actual value. The effect

of M and N on the system eigenvalue are shown in Fig. (26). It can be seen from the figure that as the number of terms increases, the buckling load decreases till reaching a steady value. For M this steady value happens to be around 18, and for N around 13. If too few terms are used in the series, then the solution of the eigenvalue problem seems to be unstable, producing unreasonably high or low values for the eigenvalues (thus for the buckling loads).

Increasing M and N increases the accuracy of the results obtained in the buckling analysis. However, these parameters increase the size of the problem as well, thus increasing the time it takes for a single run to be completed. The graph presented on the right hand side of Fig.(26) shows the variation of the time required for the completion of each run on an RS 6000 machine with respect to M . As can be seen, computer time increases proportional to the value of M . In order to save computer time and do more analyses per hour for better optimization results, we would like to keep the values of the convergence parameters as low as possible without compromising much on the accuracy of the results.

To obtain reasonable results M and N need to be above certain values. As a rule of thumb these values can be determined by counting the number of grid cells along both panel axes and multiplying these numbers by two. We chose to multiply by two because we want to make sure that the skin can buckle locally in a double sine wave within each grid cell.

7.3.2 Influence of K and K'

Parameter K controls the number of constraint points along the stiffener axes. At these constraint points, both out-of-plane deflection and rotation constraints are imposed on the problem. The smaller the number of K , the less the number of constraints are and the higher the degree of freedom is for the system. Therefore, small K values lead to small buckling loads, leading to conservative designs.

Variation of the smallest eigenvalue of the system with respect to K is given in Fig. (27). It can be seen that increasing K introduces more constraint points into the problem, making the analytical model of the problem more similar to the real case, and as a consequence the eigenvalue increases with increasing K .

Just like there is a rule of thumb for determining the minimum values of M and N for acceptable results, there is a rule to determine the minimum number of constraint points on each stiffener. This rule can be stated as; on each stiffener, there should be at least twice as many constraints points as the number of stiffeners crossing that particular stiffener. Looking at Fig. (27), we can see that choosing 15 constraint points on each stiffener gives us a convergent result. However, to conduct faster analyses, K can be chosen as 10 which causes a loss of accuracy by 6%.

The parameter K' represents the number of terms in the out-of-plane deflection function of the stiffeners. As it was for the terms M and N , the larger this parameter is, the more accurate is the solution to the buckling analysis. However, the minimum value of this parameter is sought for an acceptable solution. Upon plotting the effect of K' in Fig. (27), it is seen that there are two regions of stability in the graph. The first region is between $K'=5$ and $K'=16$ where we see a constant value of 0.72 for the eigenvalue. The second region is for K' values greater than 17 where the eigenvalue has a lower value of 0.61. We can either chose $K'=17$ and sacrifice computer time by 40% or we can choose $K'=6$, and sacrifice the accuracy by 15%. For optimization purposes we would rather use $K'=6$ to do more analyses in a given period of time, despite the fact that there will be some loss of accuracy.

The convergence study presented here is carried out to determine how many terms are needed in the Fourier series that are used in modeling of the panel. It should be noticed that as the number of terms are increased, the system eigenvalue converges to a certain value. Appropriate values obtained for the 4 convergence parameters are specific to this panel configuration and are likely to change with

different panel geometries. So, it would be a good idea to conduct similar convergence studies in case of working with different panel configurations before proceeding with optimization.

7.4 Parametric Studies On Panel Buckling

In this chapter we aim to see how does the skin and stiffener stacking sequences change the grid-stiffened panel's resistance to thermal buckling. We will not specify whether the panel is cooled or heated since both types of thermal loads are experienced by the space structures. What we will be interested in is the magnitude of these loads, i.e., the temperature range that the space structure can function without buckling.

A grid-stiffened panel having stiffeners on both sides with 5 pair of stiffeners oriented at ± 39 degrees is considered. The top view of the panel is provided in Fig. 25. All edges of the panel are restrained, neither the number of stiffeners nor the stiffener orientations are varied. Only variables are the skin and the stiffener stacking sequences. Using different stacking sequences for the skin and stiffener laminates, we try to determine the thermal loads that cause panel buckling.

Numeric results are provided in Tables 3 and 4 for different stiffener and skin stacking sequences. Even though the stacking sequence and number of plies are changed, the total thickness of the skin and the stiffener laminates are kept constant at 4×10^{-2} and 3×10^{-2} inches as respectively.

Table 3 shows the results obtained for a grid-stiffened panel with a skin stacking sequence of $[0/\pm 45/90]_s$. It can be seen that putting ± 45 plies into the stiffener stacking sequence rather than using all 0 degree plies, increases the thermal buckling load of the panel. This is due to the fact that ± 45 plies decrease the stiffener's expansion tendency without compromising its bending stiffness considerably. Comparing the third and fourth rows of this table, we can say that using 90° plies rather than 0° in the stiffener laminates gives us higher panel thermal buckling loads. However, we

Stiffener Stacking Sequence	Applied Temperature Difference ($^{\circ}$ F)	Longitudinal CTE (F^{-1})
$[0]_s$	-37	-6.4×10^{-7}
$[\pm 45]_s$	-39.2	-3.28×10^{-7}
$[0/\pm 45]_s$	-37.7	-7.31×10^{-7}
$[\pm 45/90]_s$	-38.8	4.57×10^{-7}
$[90]_s$	-11.5	17.2×10^{-7}

Table 3: Variation of Panel Thermal Buckling Load For Different Stiffener Stacking Sequences, With a $[0/\pm 45/90]_s$ Laminate Skin

see that stiffener laminates made of all 90° plies decrease the buckling load to a great extent when compared to the applied temperature difference obtained for stiffener laminates with all 0° plies. It can be deduced that while the 0° plies contribute to the stiffener bending stiffness the most, they also increase the stiffener's expansion tendency upon cooling. The opposite is valid for 90 degree plies, i.e., they decrease the stiffener's expansion behavior due to their shrinking characteristic, but also decrease the bending stiffness as well. It looks like higher thermal buckling loads can be obtained for panels with stiffeners possessing low thermal expansion coefficients and high bending stiffnesses. Theoretically, this can be achieved by tailoring the stiffener laminates.

Table 4 includes the results obtained for a grid-stiffened panel with different skin stacking sequences, and with stiffeners made of $[\pm 45]_s$ laminates. Varying the skin stacking sequence has a different effect on the panel response than varying the stiffener stacking sequence. As was mentioned earlier, and as was shown in Fig. (15), the grid layer deforms like an isotropic material under thermal loads regardless of the stiffeners' stacking sequence. On the other hand, depending on its thermal and stiffness properties, the skin directly contributes to the isotropy or anisotropy of the panel. Looking at this table we see that the skin laminates with some 90° plies in them cause low thermal buckling

Skin Stacking Sequence	Applied Temperature Difference ($^{\circ}$ F)
$[\pm 45]_s$	-44.2
$[0_2 / \pm 45]_s$	-52
$[\pm 45 / 90_2]_s$	-36.8
$[0 / \pm 45 / 90]_s$	-37.7
$[0 / \pm 45]_s$	-48
$[\pm 45 / 90]_s$	-37.3
$[0]_s$	+17

Table 4: Variation of Panel Thermal Buckling Load For Different Skin Stacking Sequences, With $[\pm 45]_s$ Stiffeners

loads for the panel; which may suggest that lower bending stiffness values associated with the 90° plies in skin stacking sequence hinders the panel's ability to carry higher thermal loads. Indeed, when only cooling is considered, the panel which has its skin made of a $[\pm 45 / 90_2]_s$ laminate has the lowest thermal buckling load in the table with $\Delta T = -36.8^{\circ}$ F. On the other hand, when a skin laminate includes some amount of 0° plies, it is seen that it causes a higher panel buckling load than the former type. For example, a skin with the stacking sequence of $[0_2 / \pm 45]_s$ causes the highest panel thermal buckling load with $\Delta T = -52^{\circ}$.

When a skin laminate made of all 0° plies is employed in the panel, it is seen that the panel thermal buckling load comes out positive. This means that such a panel will not buckle under cooling but upon heating. A laminate made of all 0° plies has thermal expansion coefficients of -6.4×10^{-7} and 1.72×10^{-5} along the x and y coordinate axes respectively. A negative thermal expansion coefficient creates compression and a positive thermal expansion coefficient creates tension along the restrained skin edges upon cooling. So, the all- 0° -plies-skin is experiencing compression along the x-axis and

tension along the y-axis. It should be noted that the energy equation determining the buckling load includes both of these loads (N_x, N_y). In this case these loads have opposite signs, and the effect of N_y outweighs the effect of N_x . Therefore, cooling the panel does not cause it to buckle. In many space applications, structures go through cyclic thermal loads, such as heating and cooling following each other. From this perspective it can be said that the last panel configuration we have considered, i.e., with a skin made of all 0° plies will not be very desirable for cyclic loading (in addition to its undesirable failure characteristics), since during heating it will buckle at a temperature change of $+17^\circ$ F.

To increase the thermal buckling load of a grid-stiffened panel we need to minimize the thermal expansion or contraction coefficients of the structure along both x and y coordinate axes. It was already mentioned that the thermal expansion coefficient of a grid layer was the same along both panel axes and was equal to the longitudinal thermal expansion coefficient of a stiffener. Minimizing the stiffeners' longitudinal expansion coefficients without compromising their bending stiffness too much can be the first step to be taken to increase the thermal buckling load of a panel. Minimizing the thermal expansion coefficients of the skin would be the second step, which is just like of any composite laminate's and was discussed in Chapter 3.1.1. It should be noted that obtaining zero thermal expansion coefficients for every laminate used in the panel would be the ideal for our purpose, however, considering the material properties of P-100 graphite-epoxy material we have been using, this is not quite possible (see Eq. 41).

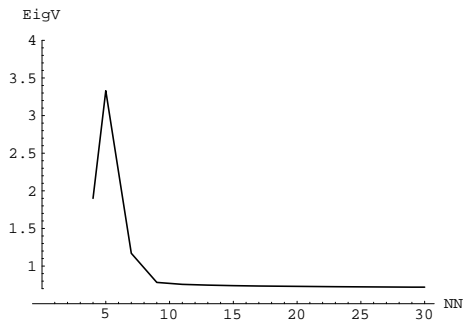
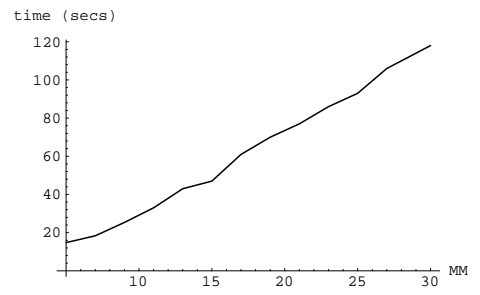
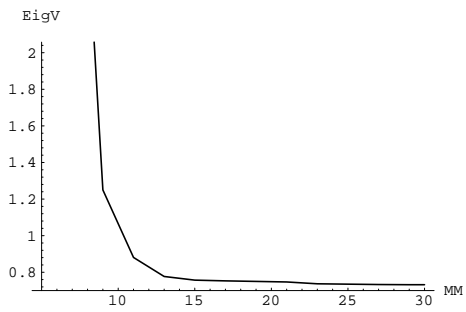


Figure 26: Effect of skin out-of-plane deflection terms on the system eigenvalue and on the computer time

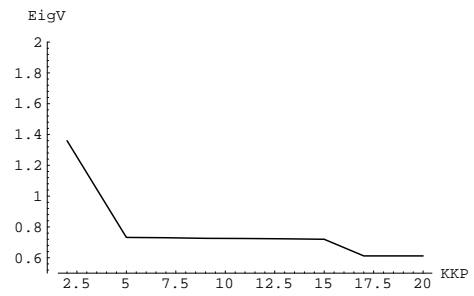
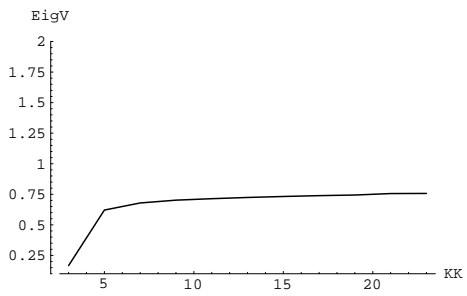


Figure 27: Effect of stiffener out-of-plane deflection terms on the system eigenvalue

8 Conclusions

This study was aimed at developing an analysis capability for the thermal deformation response and thermal buckling of grid-stiffened composite panels. To accomplish this goal, an approach incorporating several different concepts was undertaken. These concepts consist of; thermal deformation response of composite laminates, thermal deformation response of grid-stiffened panels, and thermal buckling analysis of grid-stiffened panels.

Deformation response of composite laminates under uniform thermal loads was presented in Chapter 2. To help us measure the laminates' response two thermal coefficient vectors were introduced, namely the thermal expansion coefficient and the thermal bending coefficient. In Chapter 3.1.1 the criteria for a composite laminate to deform like an isotropic material was given. An equation based solely on the ply level material properties of a composite material was derived in Chapter 3.1.2 to obtain laminates with no in-plane thermal deformations. As a result of this part of the study it was demonstrated that for a symmetric composite laminate to behave isotropically under thermal loads, it had to possess a zero V_1^* in-plane stiffness term. For a symmetric and balanced laminate to show no in-plane deformations under uniform thermal loading, its material properties had to satisfy an equation derived in the thesis Eq. (41). Numerical and graphical results for thermal expansion and thermal bending coefficients of laminates with different patterns of stacking sequences were illustrated in Chapter 3.2. It was shown that under uniform thermal loads, unsymmetric laminates experienced both curvature and in-plane deformations. On the other hand, symmetric laminates did not experience any curvatures under the same conditions. In-plane shear deformation as a result of uniform thermal loading was seen in laminates with unbalanced stacking sequences.

After investigating the thermal response of composite laminates, Chapter 6 combined the stiffness

and thermal properties of the skin and the stiffener laminates forming the panel. Graphical results were presented to show the variation of panel deformations with respect to different panel parameters. An unrestrained panel with stiffeners on one side experienced curvatures in both panel directions upon thermal loading. Amount of these curvatures were dependent on the stiffeners' thermal and stiffness properties, as well as their orientation. Grid height was shown to have an effect on the magnitude of panel curvatures but not on their nature. Changing the stiffeners' stacking sequence has changed the thermal expansion and bending characteristics of the panel. When the stiffener stacking sequence was chosen in such a way that the grid layer and the skin had the same thermal expansion coefficients along both panel axes, the panel remained flat under uniform thermal loads. A good example for this case was a panel with its skin and stiffener laminates made of quasi-isotropic laminates, i.e., laminates with $[0/\pm 45/90]_s$ stacking sequence.

For conditions where the panel undergoing thermal loading had restrained edges, suppressed deformations created in-plane loads on the skin and the stiffeners. When in-plane loads acting on the skin and stiffener laminates were compressive, these members carried the risk of failing under buckling. Therefore, in Chapter 6.6 we have introduced the equations governing the thermal buckling of composite laminates. Also in the same chapter an overview of the global panel buckling analysis was given. Chapter 7.4 presented some numerical results on the thermal buckling loads of grid-stiffened panels with various skin and stiffener stacking sequences. It was seen that a panel which had $[\pm 45]_s$ laminates for its stiffeners and a $[0_2/\pm 45]_s$ laminate for its skin had the highest thermal buckling load among all the others considered. As a result, it was concluded that a panel with restrained edges, made of laminates possessing almost zero thermal expansion coefficients would be the most stable under uniform thermal loads regardless of the thermal loads' nature.

This last statement also emphasizes the importance of Chapter 3. It can be also noticed that,

all the concepts mentioned earlier in this conclusion chapter are interrelated with one and other, and the results obtained at the end of each chapter contributes to our understanding of the thermal deformation response and thermal buckling analysis of grid-stiffened composite panels.

B Stiffness Terms

$$\begin{aligned}\check{A} &= \frac{\mathbf{A}}{\text{DEN}} \\ \check{B} &= \frac{\mathbf{B}}{\text{DEN}} \\ \check{D} &= \frac{\mathbf{D}}{\text{DEN}}\end{aligned}$$

where \mathbf{A} , \mathbf{B} , \mathbf{D} and DEN are given in terms of the stiffness properties of the stiffener laminates as;

$$\begin{aligned}\mathbf{A} &= A_{66} B_{16}^2 B_{22}^2 - 2 A_{66} B_{12} B_{16} B_{22} B_{26} - 2 A_{26} B_{16}^2 B_{22} B_{26} + A_{66} B_{12}^2 B_{26}^2 + 2 A_{26} B_{12} B_{16} B_{26}^2 + \\ &A_{22} B_{16}^2 B_{26}^2 + 2 A_{16} B_{16} B_{22} B_{26}^2 - 2 A_{16} B_{12} B_{26}^3 - 2 A_{12} B_{16} B_{26}^3 + A_{11} B_{26}^4 + A_{22} B_{12}^2 B_{66}^2 + \\ &2 A_{26} B_{12} B_{16} B_{22} B_{66} - 2 A_{16} B_{16} B_{22}^2 B_{66} - 2 A_{26} B_{12}^2 B_{26} B_{66} - 2 A_{22} B_{12} B_{16} B_{26} B_{66} + \\ &2 A_{16} B_{12} B_{22} B_{26} B_{66} + 2 A_{12} B_{16} B_{22} B_{26} B_{66} + 2 A_{12} B_{12} B_{26}^2 B_{66} - 2 A_{11} B_{22} B_{26}^2 B_{66} - \\ &2 A_{12} B_{12} B_{22} B_{66}^2 + A_{11} B_{22}^2 B_{66}^2 + A_{26}^2 B_{16}^2 D_{22} - A_{22} A_{66} B_{16}^2 D_{22} - 2 A_{16} A_{26} B_{16} B_{26} D_{22} + \\ &2 A_{12} A_{66} B_{16} B_{26} D_{22} + A_{16}^2 B_{26}^2 D_{22} - A_{11} A_{66} B_{26}^2 D_{22} + 2 A_{16} A_{22} B_{16} B_{66} D_{22} - \\ &2 A_{12} A_{26} B_{16} B_{66} D_{22} - 2 A_{12} A_{16} B_{26} B_{66} D_{22} + 2 A_{11} A_{26} B_{26} B_{66} D_{22} + A_{12}^2 B_{66}^2 D_{22} - \\ &A_{11} A_{22} B_{66}^2 D_{22} - 2 A_{26}^2 B_{12} B_{16} D_{26} + 2 A_{22} A_{66} B_{12} B_{16} D_{26} + 2 A_{16} A_{26} B_{16} B_{22} D_{26} - \\ &2 A_{12} A_{66} B_{16} B_{22} D_{26} + 2 A_{16} A_{26} B_{12} B_{26} D_{26} - 2 A_{12} A_{66} B_{12} B_{26} D_{26} - 2 A_{16} A_{22} B_{16} B_{26} D_{26} + \\ &2 A_{12} A_{26} B_{16} B_{26} D_{26} - 2 A_{16}^2 B_{22} B_{26} D_{26} + 2 A_{11} A_{66} B_{22} B_{26} D_{26} + 2 A_{12} A_{16} B_{26}^2 D_{26} - \\ &2 A_{11} A_{26} B_{26}^2 D_{26} - 2 A_{16} A_{22} B_{12} B_{66} D_{26} + 2 A_{12} A_{26} B_{12} B_{66} D_{26} + 2 A_{12} A_{16} B_{22} B_{66} D_{26} - \\ &2 A_{11} A_{26} B_{22} B_{66} D_{26} - 2 A_{12}^2 B_{26} B_{66} D_{26} + 2 A_{11} A_{22} B_{26} B_{66} D_{26} + A_{16}^2 A_{22} D_{26}^2 + A_{11} A_{26}^2 D_{26}^2 - \\ &2 A_{12} A_{16} A_{26} D_{26}^2 + A_{12}^2 A_{66} D_{26}^2 - A_{11} A_{22} A_{66} D_{26}^2 + A_{26}^2 B_{12}^2 D_{66} - A_{22} A_{66} B_{12}^2 D_{66} - \\ &2 A_{16} A_{26} B_{12} B_{22} D_{66} + 2 A_{12} A_{66} B_{12} B_{22} D_{66} - A_{11} A_{66} B_{22}^2 D_{66} + 2 A_{16} A_{22} B_{12} B_{26} D_{66} -\end{aligned}$$

$$\begin{aligned}
& 2 A_{12} A_{26} B_{12} B_{26} D_{66} - 2 A_{12} A_{16} B_{22} B_{26} D_{66} + 2 A_{11} A_{26} B_{22} B_{26} D_{66} + A_{12}^2 B_{26}^2 D_{66} - \\
& A_{11} A_{22} B_{26}^2 D_{66} - A_{16}^2 A_{22} D_{22} D_{66} + 2 A_{12} A_{16} A_{26} D_{22} D_{66} - A_{11} A_{26}^2 D_{22} D_{66} + A_{16}^2 B_{22}^2 D_{66} - \\
& A_{12}^2 A_{66} D_{22} D_{66} + A_{11} A_{22} A_{66} D_{22} D_{66}
\end{aligned}$$

$$\begin{aligned}
\mathbf{B} = & B_{16}^2 B_{22} B_{26}^2 - 2 B_{12} B_{16} B_{26}^3 + B_{11} B_{26}^4 - B_{16}^2 B_{22}^2 B_{66} + 2 B_{12} B_{16} B_{22} B_{26} B_{66} + B_{12}^2 B_{26}^2 B_{66} - \\
& 2 B_{11} B_{22} B_{26}^2 B_{66} - B_{12}^2 B_{22} B_{66}^2 + B_{11} B_{22}^2 B_{66}^2 - A_{66} B_{16} B_{22} B_{26} D_{12} + A_{66} B_{12} B_{26}^2 D_{12} + \\
& A_{26} B_{16} B_{26}^2 D_{12} - A_{16} B_{26}^3 D_{12} + A_{26} B_{16} B_{22} B_{66} D_{12} - 2 A_{26} B_{12} B_{26} B_{66} D_{12} - A_{12} B_{26}^3 D_{16} - \\
& A_{22} B_{16} B_{26} B_{66} D_{12} + A_{16} B_{22} B_{26} B_{66} D_{12} + A_{12} B_{26}^2 B_{66} D_{12} + A_{22} B_{12} B_{66}^2 D_{12} - \\
& A_{12} B_{22} B_{66}^2 D_{12} + A_{66} B_{16} B_{22}^2 D_{16} - A_{66} B_{12} B_{22} B_{26} D_{16} - 2 A_{26} B_{16} B_{22} B_{26} D_{16} + \\
& A_{26} B_{12} B_{26}^2 D_{16} + A_{22} B_{16} B_{26}^2 D_{16} + A_{16} B_{22} B_{26}^2 D_{16} + A_{26} B_{12} B_{22} B_{66} D_{16} - A_{16} B_{22}^2 B_{66} D_{16} - \\
& A_{22} B_{12} B_{26} B_{66} D_{16} + A_{12} B_{22} B_{26} B_{66} D_{16} + A_{66} B_{12} B_{16} B_{26} D_{22} - A_{26} B_{16}^2 B_{26} D_{22} - \\
& A_{66} B_{11} B_{26}^2 D_{22} + A_{16} B_{16} B_{26}^2 D_{22} - A_{26} B_{12} B_{16} B_{66} D_{22} + A_{22} B_{16}^2 B_{66} D_{22} + A_{12} B_{12} B_{66}^2 D_{22} - \\
& A_{16} B_{12} B_{26} B_{66} D_{22} + 2 A_{26} B_{11} B_{26} B_{66} D_{22} - A_{12} B_{16} B_{26} B_{66} D_{22} - A_{22} B_{11} B_{66}^2 D_{22} + \\
& A_{26}^2 B_{16} D_{16} D_{22} - A_{22} A_{66} B_{16} D_{16} D_{22} - A_{16} A_{26} B_{26} D_{16} D_{22} + A_{12} A_{66} B_{26} D_{16} D_{22} + \\
& A_{16} A_{22} B_{66} D_{16} D_{22} - A_{12} A_{26} B_{66} D_{16} D_{22} - A_{66} B_{12} B_{16} B_{22} D_{26} + A_{26} B_{16}^2 B_{22} D_{26} - \\
& A_{66} B_{12}^2 B_{26} D_{26} + 2 A_{26} B_{12} B_{16} B_{26} D_{26} - A_{22} B_{16}^2 B_{26} D_{26} + 2 A_{66} B_{11} B_{22} B_{26} D_{26} - \\
& 2 A_{16} B_{16} B_{22} B_{26} D_{26} - 2 A_{26} B_{11} B_{26}^2 D_{26} + A_{16} B_{12} B_{26}^2 D_{26} + A_{12} B_{16} B_{26}^2 D_{26} + \\
& A_{26} B_{12}^2 B_{66} D_{26} - A_{22} B_{12} B_{16} B_{66} D_{26} - 2 A_{26} B_{11} B_{22} B_{66} D_{26} + A_{16} B_{12} B_{22} B_{66} D_{26} + \\
& A_{12} B_{16} B_{22} B_{66} D_{26} + 2 A_{22} B_{11} B_{26} B_{66} D_{26} - 2 A_{12} B_{12} B_{26} B_{66} D_{26} - A_{26}^2 B_{16} D_{12} D_{26} + \\
& A_{22} A_{66} B_{16} D_{12} D_{26} + A_{16} A_{26} B_{26} D_{12} D_{26} - A_{12} A_{66} B_{26} D_{12} D_{26} - A_{16} A_{22} B_{66} D_{12} D_{26} +
\end{aligned}$$

$$\begin{aligned}
& A_{12} A_{26} B_{66} D_{12} D_{26} - A_{26}^2 B_{12} D_{16} D_{26} + A_{22} A_{66} B_{12} D_{16} D_{26} + A_{16} A_{26} B_{22} D_{16} D_{26} - \\
& A_{12} A_{66} B_{22} D_{16} D_{26} - A_{16} A_{22} B_{26} D_{16} D_{26} + A_{12} A_{26} B_{26} D_{16} D_{26} + A_{26}^2 B_{11} D_{26}^2 - \\
& A_{22} A_{66} B_{11} D_{26}^2 - A_{16} A_{26} B_{12} D_{26}^2 + A_{12} A_{66} B_{12} D_{26}^2 + A_{16} A_{22} B_{16} D_{26}^2 - A_{12} A_{26} B_{16} D_{26}^2 + \\
& A_{66} B_{12}^2 B_{22} D_{66} - A_{26} B_{12} B_{16} B_{22} D_{66} - A_{66} B_{11} B_{22}^2 D_{66} + A_{16} B_{16} B_{22}^2 D_{66} - A_{26} B_{12}^2 B_{26} D_{66} + \\
& A_{22} B_{12} B_{16} B_{26} D_{66} + 2 A_{26} B_{11} B_{22} B_{26} D_{66} - A_{16} B_{12} B_{22} B_{26} D_{66} - A_{12} B_{16} B_{22} B_{26} D_{66} - \\
& A_{22} B_{11} B_{26}^2 D_{66} + A_{12} B_{12} B_{26}^2 D_{66} + A_{26}^2 B_{12} D_{12} D_{66} - A_{22} A_{66} B_{12} D_{12} D_{66} - A_{26}^2 B_{11} D_{22} D_{66} - \\
& A_{16} A_{26} B_{22} D_{12} D_{66} + A_{12} A_{66} B_{22} D_{12} D_{66} + A_{16} A_{22} B_{26} D_{12} D_{66} - A_{12} A_{26} B_{26} D_{12} D_{66} + \\
& A_{22} A_{66} B_{11} D_{22} D_{66} + A_{16} A_{26} B_{12} D_{22} D_{66} - A_{12} A_{66} B_{12} D_{22} D_{66} - A_{16} A_{22} B_{16} D_{22} D_{66} + \\
& A_{12} A_{26} B_{16} D_{22} D_{66}
\end{aligned}$$

$$\begin{aligned}
\mathbf{D} = & B_{26}^4 D_{11} - 2 B_{22} B_{26}^2 B_{66} D_{11} + B_{22}^2 B_{66}^2 D_{11} - 2 B_{16} B_{26}^3 D_{12} + 2 B_{16} B_{22} B_{26} B_{66} D_{12} + \\
& 2 B_{12} B_{26}^2 B_{66} D_{12} - 2 B_{12} B_{22} B_{66}^2 D_{12} + A_{66} B_{26}^2 D_{12}^2 - 2 A_{26} B_{26} B_{66} D_{12}^2 + A_{22} B_{66}^2 D_{12}^2 + \\
& 2 B_{16} B_{22} B_{26}^2 D_{16} - 2 B_{12} B_{26}^3 D_{16} - 2 B_{16} B_{22}^2 B_{66} D_{16} + 2 B_{12} B_{22} B_{26} B_{66} D_{16} - \\
& 2 A_{66} B_{22} B_{26} D_{12} D_{16} + 2 A_{26} B_{26}^2 D_{12} D_{16} + 2 A_{26} B_{22} B_{66} D_{12} D_{16} - 2 A_{22} B_{26} B_{66} D_{12} D_{16} + \\
& A_{66} B_{22}^2 D_{16}^2 - 2 A_{26} B_{22} B_{26} D_{16}^2 + A_{22} B_{26}^2 D_{16}^2 + B_{16}^2 B_{26}^2 D_{22} - 2 B_{12} B_{16} B_{26} B_{66} D_{22} + \\
& B_{12}^2 B_{66}^2 D_{22} - A_{66} B_{26}^2 D_{11} D_{22} + 2 A_{26} B_{26} B_{66} D_{11} D_{22} - A_{22} B_{66}^2 D_{11} D_{22} + \\
& 2 A_{66} B_{12} B_{26} D_{16} D_{22} - 2 A_{26} B_{16} B_{26} D_{16} D_{22} - 2 A_{26} B_{12} B_{66} D_{16} D_{22} + A_{26}^2 D_{16}^2 D_{22} + \\
& 2 A_{22} B_{16} B_{66} D_{16} D_{22} - A_{22} A_{66} D_{16}^2 D_{22} - 2 B_{16}^2 B_{22} B_{26} D_{26} + 2 B_{12} B_{16} B_{26}^2 D_{26} + \\
& 2 B_{12} B_{16} B_{22} B_{66} D_{26} - 2 B_{12}^2 B_{26} B_{66} D_{26} + 2 A_{66} B_{22} B_{26} D_{11} D_{26} - 2 A_{26} B_{26}^2 D_{11} D_{26} - \\
& 2 A_{26} B_{22} B_{66} D_{11} D_{26} + 2 A_{22} B_{26} B_{66} D_{11} D_{26} - 2 A_{66} B_{12} B_{26} D_{12} D_{26} + 2 A_{26} B_{16} B_{26} D_{12} D_{26} + \\
& 2 A_{26} B_{12} B_{66} D_{12} D_{26} - 2 A_{22} B_{16} B_{66} D_{12} D_{26} - 2 A_{66} B_{12} B_{22} D_{16} D_{26} + 2 A_{26} B_{16} B_{22} D_{16} D_{26} +
\end{aligned}$$

$$\begin{aligned}
& 2 A_{26} B_{12} B_{26} D_{16} D_{26} - 2 A_{22} B_{16} B_{26} D_{16} D_{26} - 2 A_{26}^2 D_{12} D_{16} D_{26} + 2 A_{22} A_{66} D_{12} D_{16} D_{26} + \\
& A_{66} B_{12}^2 D_{26}^2 - 2 A_{26} B_{12} B_{16} D_{26}^2 + A_{22} B_{16}^2 D_{26}^2 + A_{26}^2 D_{11} D_{26}^2 - A_{22} A_{66} D_{11} D_{26}^2 + \\
& B_{16}^2 B_{22}^2 D_{66} - 2 B_{12} B_{16} B_{22} B_{26} D_{66} + B_{12}^2 B_{26}^2 D_{66} - A_{66} B_{22}^2 D_{11} D_{66} + A_{22} A_{66} D_{11} D_{22} D_{66} \\
& 2 A_{26} B_{22} B_{26} D_{11} D_{66} - A_{22} B_{26}^2 D_{11} D_{66} + 2 A_{66} B_{12} B_{22} D_{12} D_{66} - 2 A_{26} B_{16} B_{22} D_{12} D_{66} - \\
& 2 A_{26} B_{12} B_{26} D_{12} D_{66} + 2 A_{22} B_{16} B_{26} D_{12} D_{66} + A_{26}^2 D_{12}^2 D_{66} - A_{22} A_{66} D_{12}^2 D_{66} - \\
& A_{66} B_{12}^2 D_{22} D_{66} + 2 A_{26} B_{12} B_{16} D_{22} D_{66} - A_{22} B_{16}^2 D_{22} D_{66} - A_{26}^2 D_{11} D_{22} D_{66}
\end{aligned}$$

$$\begin{aligned}
\mathbf{DEN} = & B_{26}^4 - 2 B_{22} B_{26}^2 B_{66} + B_{22}^2 B_{66}^2 - A_{66} B_{26}^2 D_{22} + 2 A_{26} B_{26} B_{66} D_{22} - \\
& A_{22} B_{66}^2 D_{22} + 2 A_{66} B_{22} B_{26} D_{26} - 2 A_{26} B_{26}^2 D_{26} - 2 A_{26} B_{22} B_{66} D_{26} + \\
& 2 A_{22} B_{26} B_{66} D_{26} + A_{26}^2 D_{26}^2 - A_{22} A_{66} D_{26}^2 - A_{66} B_{22}^2 D_{66} + \\
& 2 A_{26} B_{22} B_{26} D_{66} - A_{22} B_{26}^2 D_{66} - A_{26}^2 D_{22} D_{66} + A_{22} A_{66} D_{22} D_{66}
\end{aligned}$$

C SPANDO Input File

C***** DESIGN OF GEODESICALLY STIFFENED PANELS DATA FILE *****

C

C Data file format: Input value, Variable representation - Definition

C

C

C** SKIN/STIFFENER CONTINUITY AND PANEL ANALYSIS ASSUMPTIONS **

C

2 ROTATE - 1:Deformation continuity; 2:Rotation and deformation continuity

2 NTRANS - Stiffener transverse condition 1:eps-zeta=0; 2:N-zeta=0

2 ANTYP- Analysis type

0 NEPSX - Panel edge condition

0 NEPSY - Panel edge condition

C 1:eps-x=0 (applied load in x dir. is assumed to be zero);

C 2:eps-x not 0 (biaxial loads)

C

C

C** PANEL DIMENSIONS (inches) **

C

70.D+00 PL - Panel length (X)

25.D+00 PH - Panel height (Y)

C

C

C PANEL LOADING CONDITIONS ****

C

C (Positive is compression; Units are lbs/in)

C

00.0D+00 PNX - X direction loading

00.D+00 PNY - Y direction loading

00.D+00 PNX Y - Shear loading

-50.D+00 DELT - Temperature Difference

C

C

C SKIN ELASTIC PROPERTIES ****

C

53.5D+06 E(1,1) - Young's Modulus (E1 psi)

0.73D+06 E(1,2) - Young's Modulus (E2 psi)

0.76D+06 E(1,3) - Shear Modulus (G12 psi)

0.31D+00 E(1,4) - Major Poisson's Ratio (ν_{12})

0.062D+00 E(1,5) - Material density

-0.64D-06 E(1,6) - Thermal Expansion Coeff. in fiber direction

17.2D-06 E(1,7) - Thermal Expansion Coeff. in matrix direction

C

C

C SKIN ALLOWABLE STRAIN ****

C

0.81D-03 EALL(1,1) - Epsilon-1 (compression)

2.21D-03 EALL(1,2) - Epsilon-1 (tension)

9.0D-03 EALL(1,3) - Epsilon-2 (compression)

2.67D-03 EALL(1,4) - Epsilon-2 (tension)

4.039D-03 EALL(1,5) - Gamma-12 (shear)

C

C

C** SKIN LAYUP **

C

C Symmetry assumed, input half of stacking sequence only.

C First ply represents outer most ply in laminate.

C

4 NHPLYS - Number of plies in the skin

C

C Column 1: J - Skin ply number

C Column 2: THIK(1,J) - Thickness of skin ply J (along Z axes)

C Column 3: THETA(1,J) - Angle orientation of skin ply J

C

1 0.500000D-02 0.D+00

2 0.500000D-02 45.D+00

3 0.500000D-02 -45.D+00

4 0.500000D-02 90.D+00

C

C

C SKIN OUT-OF-PLANE DISPLACEMENT (w) SERIES TERMS ****

C

25 MM - (X-direction)

18 NN - (Y-direction)

C

C

C STIFFENER ELASTIC PROPERTIES ****

C

53.5D+06 E(1,1) - Young's Modulus (E1 psi)

0.73D+06 E(1,2) - Young's Modulus (E2 psi)

0.76D+06 E(1,3) - Shear Modulus (G12 psi)

0.31D+00 E(1,4) - Major Poisson's Ratio (v12)

0.062D+00 E(1,5) - Material density

-0.64D-06 E(1,6) - Thermal Expansion Coeff. in fiber direction

17.2D-06 E(1,7) - Thermal Expansion Coeff. in matrix direction

0.54D+06 G23R - Transverse Shear Modulus (G23 psi)

0.87D+06 G31R - Transverse Shear Modulus (G31 psi)

C

C

C STIFFENER ALLOWABLE STRAINS**

C

0.81D-03 EALL(2,1) - Epsilon-1 (compression)

2.21D-03 EALL(2,2) - Epsilon-1 (tension)

9.0D-03 EALL(2,3) - Epsilon-2 (compression)

2.67D-03 EALL(2,4) - Epsilon-2 (tension)

4.039D-03 EALL(2,5) - Gamma-12 (shear)

C

C

C** STIFFENER LAYUP **

C

C Symmetry assumed, input half of stacking sequence only.

C First ply represents outer most ply in laminate.

C

C ———IMPORTANT—————

C The stiffener ply thickness given in this section is different than

C the stiffener ply thickness given in the Manufacturing Cost

C Variables section that follows (see manual for detailed explanation).

C The stiffener tow width (also in the Manufacturing Cost Variables section)

C must be an integer multiple of the stiffener ply thickness given in this

C section assuming that the tow width represents the total width

C (along the Chi axes) of the stiffener.

C

C The code will only accept a zero degree ply orientation for

C stiffener plies - NO OTHER PLY ANGLE IS PERMITTED.

C

2 Number of Stiffener Plies

C

C Column 1: J - Stiffener ply number

C Column 2: THIK(2,J) - Thickness of ply (J) (along Chi axes)

C Column 3: THETA(2,J) - Angle orientation of ply (J)

C

1 0.750D-02 90.00D+00

2 0.750D-02 90.00D+00

C

C

C** STIFFENER PHYSICAL PROPERTIES **

C

10 NSTIF - The number of stiffeners (max no. is 26)

0.50D+0 SH - Stiffener height (inches)

2 ISIDE - 1: Stiffeners on 1 side of panel

C 2: Stiffeners on both sides of panel

C

C

C** GEOMETRY FOR EACH STIFFENER**

C

C The stiffener geometry is represented in the following manner:

C

C All stiffener coordinates given in inches

C (0,0) is bottom left corner of panel

C

C Column 1: K - Stiffener number

C Column 2: X(1,K) - X1 coordinate of stiffener K

C Column 3: Y(1,K) - Y1 coordinate of stiffener K

C Column 4: X(2,K) - X2 coordinate of stiffener K

C Column 5: Y(2,K) - Y2 coordinate of stiffener K

C

C Both X1,Y1 and X2,Y2 coordinates for all stiffeners

C must be given even if the value is zero.

C Be sure to check that the data has been inputted correctly.

C

1 0 16.83151176763495 10.08724289133763 25.

2 0 0.4945353029048505 30.26172867401288 25.

3 19.56378554331185 0 50.43621445668814 25.

4 39.73827132598712 0 70. 24.50546469709516

5 59.91275710866236 0 70. 8.16848823236506

6 0 8.16848823236505 10.08724289133763 0.

7 0 24.50546469709515 30.26172867401288 0.

8 19.56378554331185 25. 50.43621445668814 0.

9 39.73827132598712 25. 70. 0.4945353029048434

10 59.91275710866236 25. 70. 16.83151176763494

C

C

C STIFFENER CROSSING POINTS ****

C

C Column 1: II - stiffener number

C Column 2: NCROSS(II) - number of stiffeners that cross stiffener (II)

C

1 1

2 3

3 3

4 3

5 1

6 1

7 3

8 3

9 3

10 1

C

C

C SKIN/STIFFENER CONSTRAINT POINTS AND STIFFENER SERIES TERMS**

C

C Column 1: J - Stiffener number

C Column 2: KK(J) - Number of constraint points for stiffener J

C - Number of series terms (Eta-direction) for

C stiffener (J's) in-plane displacement (v)

C Column 3: KKP(J) - Number of series terms (Eta-direction)

C for stiffener (J's) out-of-plane displacement (w)

C

C Note: the number of constraint points for both the stiffener

C deformation constraint and rotation constraint is the same

C

1 16 7

2 16 7

3 16 7

4 16 7

5 16 7

6 16 7

7 16 7

8 16 7

9 16 7

10 16 7

C

C

C** STOLL'S STIFFENER CRIPPLING ANALYSIS **

C

5 NWX - No. of terms for out-of-plane displacement (w) (Eta-dir)

5 NWY - No. of terms for out-of-plane displacement (w) (Zeta-dir)

3 NPXX - No. of terms for rotation displacement (Psi_x) (Eta-dir)

3 NPXY - No. of terms for rotation displacement (Psi_x) (Zeta-dir)

3 NPYX - No. of terms for rotation displacement (Psi_y) (Eta-dir)

3 NPYX - No. of terms for rotation displacement (Psi_y) (Zeta-dir)

C

C

C STIFFENER MANUFACTURING COST VARIABLES ****

C

C ———IMPORTANT—————

C Stiffener ply thickness given in this section is not the same

C as the stiffener ply thickness given in the Stiffener Layup section.

C (see manual for detailed explanation). The stiffener tow width given

C in this section must be an integer multiple of the stiffener ply

C thickness given in the Stiffener Layup section assuming that the tow

C width represents the total width (along the Chi axes) of the stiffener.

C

C

0.01D+00 PLYT - Stiffener ply thickness (along Zeta axes) (inches)

0.0625D+00 TOWW - Stiffener tow width (along Chi axes) (inches)

0.02083333D+00 SRATE - Straight fiber layup rate (seconds/in)

3.D+00 RTIME - Time to layup ramping section (seconds)

3.D+00 REPOS - Time for repositioning (seconds)

0.6D-02 PLYS - Skin ply thickness (along Z axes) (inches)

C

C

C ADS OPTIMIZATION PARAMETERS ****

C

1 INFO - Implementation parameter

C -2: Implement ADS with specified over-ride parameters defined below

C 0: Implement ADS with ADS default values

C 1: DO NOT implement ADS

C

C * ADS over-ride Parameters *

C

1 IOBJ - Type of objective function

C 1:Panel weight minimization; 2:Manufacturing cost minimization

C

3 IWKO - Number of double precision over-ride parameters

C

C Column 1: NWKOV(I) - Parameter # for over-ride parameter (I)

C Column 2: WKOVR(I) - Parameter Value for over-ride parameter (I)

C

3 -1.E-02

6 1.E-03

37 1.E-06

C

C

3 IIWKO - Number of integer over-ride parameters

C

C Column 1: NWKOV(I) - Parameter # for over-ride parameter (I)

C Column 2: WKOVR(I) - Parameter Value for over-ride parameter (I)

C

2 0

5 4

7 50

C

C

1000 IPRINT - Print control parameter

C

C

3 NDV - Number of design variables

C

C Column 1: IDV(1,1) - Identification marker for design variable #1

C Column 2: IDV(1,2) - Identification marker for design variable #2

C Column 3: IDV(1,3) - Identification marker for design variable #3

C

1 2 3

C

C * Design variable initialization *

C

C Column 1: XDV(I) - Initial value of design variable (I)

C Column 2: VLB(I) - Lower bound for design variable (I)

C Column 3: VUB(I) - Upper bound for design variable (I)

C

1.D+00 0.32D+00 2.4D+00

1.D+00 0.25D+00 1.7361D+00

1.D+00 0.625D+00 4.D+00

C

C

4 NCON - Number of constraints

9 ISTRAT - Optimization strategy

5 IOPT - Type of optimizer used

6 IONED - Type of 1-D search used

0 IGRAD - Gradient information for ADS

C 0: Gradient computations are done with forward finite difference

C 1: User supplies gradient information. (see ADS manual)

C

C

C end of input file

References

- [1] Marvin B. Dow, "The ACEE Program and Basic Composite Research at Langley Research Center (1975 to 1986); Summary and Bibliography", NASA Reference Publication 1177, October 1987.
- [2] Rehfield, L.W., Deo, R.B., and Renieri, G.D., "Continuous Filament Advanced Composite Isogrid: A Promising Structural Concept", Fibrous Composites in Structural Design Conference No:4, San Diego, 1978
- [3] Stroud, W.J., Agranoff, N., and Anderson, M.S., "Minimum Mass Design of Filamentary Composite Panels Under Combined Loads: Design Procedure Based On A Rigorous Buckling Analysis", NASA TN D-8417, July 1977.
- [4] Manuel, S. and Williams, J. G., "Buckling and Structural Efficiency of Sandwich-Blade Stiffened Composite Compression Panels", NASA TN-1269, September 1978.
- [5] Stroud, W.J., Greene, W.H. and Anderson, M.S., "Buckling Loads of Stiffened Panels Subjected to Combined Longitudinal Compression and Shear: Results Obtained With PASCO, EAL, and STAGS Computer Programs", NASA TN-2215, January 1984.
- [6] Wellington in action, Ron Mackay, Squadron/signal publications, ICC. 1986
- [7] Reddy, A.D., Valisetty, R.R., and Rehfield, L.W., "Continuous Filament Wound Composite Concepts for Aircraft Fuselage Structures", Journal of Aircraft, Vol 22, No 3, March 1985
- [8] Rehfield, L.W., and Reddy, A.D., "Damage Tolerance of Continuous Filament Composite Isogrid Structures: A Preliminary Assessment", Composite Materials, Japan-U.S. Conference, Tokyo, 1981.

- [9] Phillips, J.L., and Gürdal, Z., "Structural Analysis and Optimum Design of Geodesically Stiffened Composite Panels " CCMS-90-05, Virginia Polytechnic Institute, July 1990.
- [10] Grall, B. and Gürdal, Z., "Structural Analysis and Design of Geodesically Stiffened Composite Panels with Variable Stiffener Distribution ", CCMS-92-24, Virginia Polytechnic Institute, August 1992.
- [11] Tauchert, T.R., and Huang, N.N., "Thermal Buckling of Symmetric Angle-Ply Laminated Plates", Composite Structures 4, Volume 1, Analysis and Design Studies, Elsevier Applied Science.
- [12] Tauchert, T.R., "Thermal Buckling of Thick Antisymmetric Angle-Ply Laminates", Journal of Thermal Stresses, Volume 10, pp 113-124, 1987.
- [13] Tauchert, T.R., and Adibhatla, S., "Optimum Thermoelastic Design of Laminated Plates", Journal of Thermal Stresses, Vol. 8, 1985.
- [14] Tauchert, T.R., Jonnalagadda, K.D., and Blandford G.E., "High-Order Thermoelastic Composite Plate Theories: An Analytic Comparison", Journal of Thermal Stresses, Volume 16, pp 265-284, 1993.
- [15] Duffy, K.J., and Adali,S., "Optimal Design of Antisymmetric Hybrid Laminates Against Thermal Buckling", Journal of Thermal Stresses, Vol. 13, 1990.
- [16] Turvey, G.J., and Marshall, I.H., "Buckling and Postbuckling of Composite Plates", pp.190-226.
- [17] Whitney, J.M., "Structural Analysis of Laminated Anisotropic Plates", Technomic Publishing Inc.,1987.

- [18] Haftka, R. & Gürdal, Z., "Elements of Structural Optimization", Kluwer Academic Publishers, 1993
- [19] Miki, M., and Sugiyama, Y., "Optimum Design of Laminated Composite Plates Using Lamination Parameters", Proceedings of the AIAA/ASME/ASCE/AHS/ASC 32nd Structures, Structural Dynamics, and Materials Conference, Baltimore, MA., Part I, pp. 275-283, April, 1991.
- [20] Miki, M., "A Graphical Method for Designing Fibrous Laminated Composites with Required In-Plane Stiffness", Trans. JSCM, 9, 2, pp. 51-55, 1983.
- [21] Leissa, A.W., "Conditions for Laminated Plates to Remain Flat Under In-plane Loading", Composite Structures, 1986, pp.261-270.
- [22] Stiffened Panel Design Optimization, FORTRAN 77 Code.
- [23] Starnes, J.H., Jr.; Knight, N.F., Jr; and Rouse, M.: Postbuckling Behavior of Selected Flat Stiffened Graphite-Epoxy Panels Loaded in Compression. 23rd AIAA Structures, Structural Dynamics and Materials Conference (New Orleans, LA, May 10-12), Collection of Technical Papers, Part 1, 1982, pp. 464-478.
- [24] Rhodes, M.D.; and Mikulas, M.M., Jr.: Composite Lattice Structure. NASA TM X-72771, Sept, 1975.

VITA

Burak Uzman was born in Ankara, Turkey in 1973. He finished his high school education in Turkey. After being an exchange student in the state of Maine for a year, he was back in Turkey for college. After four years of attending to the Mechanical Engineering Dept. of Middle East Technical University in Ankara, Turkey, he graduated with a B.S. in 1995. Being fascinated by composite materials he decided to pursue a higher degree in the same field. The fall of 1995 he began his studies at Virginia Tech. This thesis is a product of the two years he devoted to the Department of Engineering Science and Mechanics and to the room 215-D of Norris Hall. He currently wants to build airplanes and fly helicopters. In the long run he is not so sure where he will be living or what career he will be in, but for sure he hopes to preserve his positive attitude.